The Mycelium as a Network

MARK D. FRICKER,[1] LUKE L. M. HEATON,[1,2]
NICK S. JONES,[2] and LYNNE BODDY[3]

[1]Department of Plant Sciences, University of Oxford, Oxford, OX1 3RB, United Kingdom;
[2]Mathematics Department, Imperial College, Queen's Gate, London SW7 2AZ, United Kingdom;
[3]Cardiff School of Biosciences, Cardiff University, Cardiff CF10 3AX, United Kingdom

ABSTRACT The characteristic growth pattern of fungal mycelia as an interconnected network has a major impact on how cellular events operating on a micron scale affect colony behavior at an ecological scale. Network structure is intimately linked to flows of resources across the network that in turn modify the network architecture itself. This complex interplay shapes the incredibly plastic behavior of fungi and allows them to cope with patchy, ephemeral resources, competition, damage, and predation in a manner completely different from multicellular plants or animals. Here, we try to link network structure with impact on resource movement at different scales of organization to understand the benefits and challenges of organisms that grow as connected networks. This inevitably involves an interdisciplinary approach whereby mathematical modeling helps to provide a bridge between information gleaned by traditional cell and molecular techniques or biophysical approaches at a hyphal level, with observations of colony dynamics and behavior at an ecological level.

INTRODUCTION

Growth as an interconnected mycelial network is characteristic of filamentous fungi and has been subject to scientific investigation since the seminal works of Buller at the start of the 20th century ([1]–[3]). We have increasingly detailed understanding of the fundamental cellular processes needed to form a network, such as hyphal tip growth ([4]), septation ([5], [6]), hyphal orientation ([7]), branching ([8]), and fusion ([9]–[13]) ([Fig. 1A and C]). In contrast, we know far less about the molecular events at the next physical scale that leads to hyphal aggregation and hyphal differentiation, and how these impact physiological processes such as long-distance resource distribution and biomass recycling. For example, while direct uptake and intrahyphal nutrient diffusion may be sufficient to sustain short-range local growth when resources are abundant ([14]), long-distance translocation is required to deliver nutrients at a sufficient rate to growing tips, particularly in fungi that form large networks on the forest floor that are too large to distribute nutrients through diffusion alone. We know little about the quantitative contribution of different potential transport pathways, such as cytoplasmic streaming, vesicle transport, growth-induced mass flow, or evaporative mass flow, to net fluxes and overall nutrient dynamics, and how they might vary between species and developmental stage ([15]–[17]). Nevertheless, the behavior of the growing mycelial network emerges from the interaction of many such processes and requires an integrated view to understand the overall impact on fungal behavior ([18]–[20]). Our understanding is further constrained by inferences drawn from a limited number of genetically tractable model filamentous species grown under laboratory conditions (abundant, evenly dispersed, low-molecular-weight resources, high relative humidity, constant light and temperature) compared with real-world conditions (patchy, recalcitrant, ephemeral resources, fluctuating temperature, light and relative humidity).
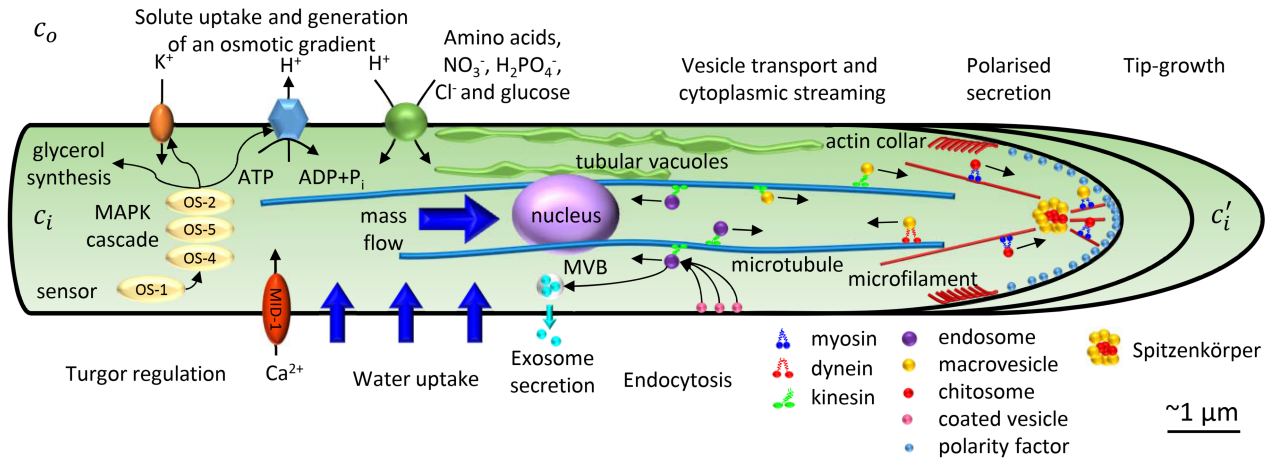
A Apical tip growth

c_o

Solute uptake and generation of an osmotic gradient

K⁺ H⁺ H⁺

Amino acids, NO_3^-, $H_2PO_4^-$, Cl⁻ and glucose

Vesicle transport and cytoplasmic streaming

Polarised secretion

Tip-growth

glycerol synthesis

ATP   ADP+P$_i$

c_i

MAPK cascade

OS-2
OS-5
OS-4

sensor OS-1

MID-1

Turgor regulation   Ca²⁺   Water uptake

tubular vacuoles

nucleus

mass flow

MVB

Exosome secretion   Endocytosis

actin collar

microtubule   microfilament

c_i'

myosin endosome Spitzenkörper
dynein macrovesicle
kinesin chitosome
coated vesicle
polarity factor

~1 µm

B Water movement in a hyphal segment

Transverse hydrostatic pressure difference from the concentration gradient of osmotically active solute inside and outside the cell (MPa)

Transverse volume flow (m³ s⁻¹)

$$\Delta P^\perp = RT(c_i - c_o)$$

$$Q_v^\perp = L_w^\perp \Delta P^\perp \pi r^2 l$$

Aquaporin Tetramer (AQP)

Hydrophobin (hp)

Longitudinal volume flow according to lamina Pouseille flow driven by the longitudinal pressure difference along the hypha due to growth (m³ s⁻¹)
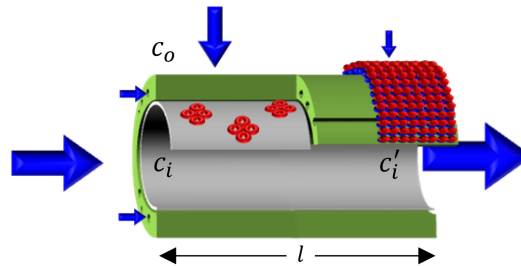
$$Q_v^\parallel = \frac{\pi r^4}{8\eta l}\Delta P^\parallel$$

Rate of water inflow per unit surface area (m s⁻¹)

$$J_v^\perp = \frac{Q_v^\perp}{\pi r^2 l} = L_w^\perp \Delta P^\perp$$

Volumetric growth rate (m³ s⁻¹)

$$\frac{dV}{dt} = Q_v^\parallel + Q_v^\perp$$

Longitudinal volume flux density (flow per unit cross-sectional area, m s⁻¹)

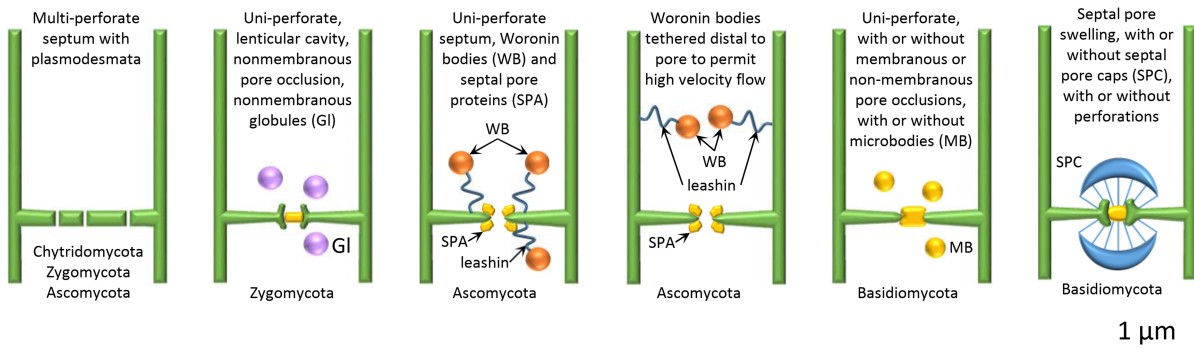$$J_v^\parallel = Q_v^\parallel \frac{1}{\pi r^2} = L_w^\parallel \Delta P^\parallel$$

c_o

c_i c_i'

l

Tip growth rate (m s⁻¹)

$$v = \frac{1}{\pi r^2}\frac{dV}{dt}$$

C Septum structure

Multi-perforate septum with plasmodesmata

Uni-perforate, lenticular cavity, nonmembranous pore occlusion, nonmembranous globules (Gl)

Uni-perforate septum, Woronin bodies (WB) and septal pore proteins (SPA)

Woronin bodies tethered distal to pore to permit high velocity flow

Uni-perforate, with or without membranous or non-membranous pore occlusions, with or without microbodies (MB)

Septal pore swelling, with or without septal pore caps (SPC), with or without perforations

Chytridomycota
Zygomycota
Ascomycota

Zygomycota   Gl

WB

SPA leashin

Ascomycota

WB leashin

SPA

Ascomycota

MB

Basidiomycota

SPC

Basidiomycota

1 µm

D Impact of septa on flow

Change in velocity through the septal pore

$$v_p = v_h \frac{r_h^2}{r_p^2}$$

r_p

Parabolic flow profile from Pouseille flow

v_p v_h

τ_p r_h

τ_h

Partial plug flow in *Neurospora*

Shear stress at the wall

$$\tau_p = \eta\frac{dv_p}{dy} \gg \tau_h = \eta\frac{dv_h}{dy}$$
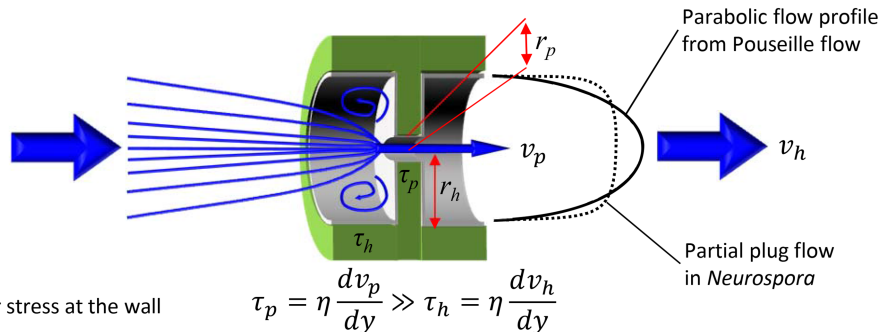
Based on Abadeh and Lew (2013), Heaton *et al.* (2012), Roper *et al.* (2016), Pieuchot *et al.* (2015)

At the whole-colony level, there is a wealth of observational data describing fungal behavior (usually of non-model but ecologically relevant species) in qualitative terms, and some progress has been made in quantitative measurements of network architecture and dynamics, in parallel with development of predictive models for network function (21–33). The challenge is to construct a framework that can integrate information across scales into a coherent model to explain fungal behavior. We start this construction process by considering the biophysical properties of the mycelial network at each scale, with particular emphasis on the interplay between the network architecture and transport of resources through the network. Most of our knowledge on network structure and dynamics comes from non-resource-unit-restricted (i.e., fungi that can extend as mycelia from their food source) wood decay basidiomycetes that forage on the forest floor for resources distributed heterogeneously in space and time (34–36). We focus on these for discussion here for this reason, and because mycorrhizal networks have been comprehensively reviewed recently (37, 38). We also examine advances in image analysis techniques to extract the network architecture, empirically based modeling and simulation techniques to predict network behavior, and experimental approaches to map the actual functional flows within the network. We finally explore how network concepts may help to define a new set of fitness traits that can be experimentally determined (39).

THE BUILDING BLOCKS FOR NETWORK CONSTRUCTION

Growth at the Hyphal Tip

The mycelial network comprises individual hyphae ranging from about 2 to 20 μm in diameter that grow by tip expansion following highly localized polar secretion of wall materials (4) (Fig. 1A). Secretory vesicles are transported to the apical cell wall using a combination of microtubule and microfilaments, powered by molecular motors such as kinesin, dynein, and myosin (4, 40–42). Excess membrane is then recycled locally by endocytosis or sorted more extensively by motile early endosomes distal from the tip (40, 41, 43). Early endosomes may also play a role as a general transport system for other cellular components, such as ribosomes and mRNA (40, 44).

Motor-driven transport of vesicles and organelles concomitantly generates cytoplasmic streaming that serves to increase the effective transport rate for solutes and other cytoplasmic components (40). This is important because the synthesis of sufficient new wall material

FIGURE 1 Mycelial network formation: tip growth and fluid flows. **(A)** Hyphae grow by extension at the tip through polarized secretion of wall materials from macrovesicles and chitosomes at the apex, choreographed by the Spitzenkörper. Membrane is recycled distal to the tip into early endosomes by endocytosis. Endosomes may also form multivesicular bodies (MVBs) that may be involved in unconventional secretion of exosomes. Transport of secretory vesicles, endosomes, and other organelles along microtubule and microfilament networks also generates cytoplasmic streaming within the apical compartment. Although wall plasticity controls hyphal extension, the driving force involves maintenance of sufficient turgor pressure by water uptake through osmosis in response to accumulation of solutes. Turgor pressure may be sensed and regulated by a mitogen-activated protein kinase (MAPK) cascade or stretch-activated channels, such as mid1. If the site of water uptake required for the volume increase during growth is distal to the tip, growth-induced mass flows will also help to move organelles and solutes toward the tip. Based on references 4, 43, 49, and 64. **(B)** Water uptake into the hypha occurs to allow tip expansion and is driven by the transverse hydrostatic pressure in response to the difference in concentration of osmotically active solutes between the medium and the hypha. The transverse hydraulic conductivity depends on the permeability of the plasma membrane and aquaporins (AQPs) in parallel, and the wall and other surface layers, such as hydrophobins, in series. Longitudinal flow in the lumen of the hypha is lamina and follows Poiseuille flow. Based on references 32, 33, 49, and 79. **(C)** Variation in septal pore structure in different fungal taxa. Redrawn from reference 96 with permission. **(D)** Impact of the septa and septal pores on fluid flows. The change in cross-sectional area causes an increase in velocity by several orders of magnitude and also increases the wall shear stress within the pore. Flow may deviate from parabolic profile expected from the Hagen-Poiseuille equation because of the density of organelles in the cytoplasm. In addition, there may be eddy currents near the pore opening that trap nuclei, vacuoles, and other organelles. Based on references 32, 65, 68, and 69.

for maximal growth requires a minimum volume of cytoplasm distal to the tip (see "Modeling tip growth and branching" below) which has to be supplied by nutrient uptake and transport, often remote from the tip ([42]). Synthesis starts with accumulation of external ions, sugars, and amino acids present in the soil or following breakdown of organic substrates, using proton-coupled cotransporters or in response to the membrane potential via ion channels ([Fig. 1A]). The low intracellular water potential from solute accumulation leads to water uptake, which is required for the increase in hyphal volume during growth, and also leads to an increase in turgor pressure. Turgor is sensed by the conserved high-osmotic glycerol (HOG) mitogen-activated protein (MAP) kinase cascade and regulates plasma-membrane ion transport ([Fig. 1A]). In addition, osmolytes such as glycerol, arabitol, other polyols, proline, or trehalose may be synthesized internally to maintain turgor ([45], [46]). Stretch-activated plasma-membrane channels, such as Mid1, may respond directly to membrane stretch and also regulate solute uptake ([Fig. 1A]). For most fungi, some minimum turgor pressure is required for tip extension, but turgor pressure *per se* does not appear to be rate limiting for normal growth, because hyphae experiencing different turgor pressures can grow at the same rate. Indeed, some fungus-like oomycetes and wall-less fungal mutants can grow in the absence of turgor pressure, when the cytoskeleton alone may be sufficient to drive the tip of the hyphae forward ([41], [47]–[50]).

Transport at the Tip

Several parallel systems contribute to solute and organelle movement within the apical and subapical compartments. In all systems, solutes will move by diffusion through the cytosol ([51], [52]) or the dynamic tubular vacuolar system ([53]–[55]), and this may be sufficient to allow bidirectional source-sink nutrient movements in slow-growing species ([56]), particularly as diffusion is constrained effectively to one dimension within the hyphae ([52], [53]), or "non-translocating" species that do not show protoplasmic streaming ([57]). For example, the time (t_D) for a species j to diffuse length l scales as l^2/D_j. Thus, ions and small molecules with a diffusion coefficient (D_j) of 1 to 2×10^{-9} m^2 s^{-1} would transit a typical apical compartment in *Phanerochaete velutina* (400 μm) in ~2 min, while proteins, with a diffusion coefficient of 2×10^{-11}, would take ~2 h. Transport over a small colony (10 mm) would take 20 h for small molecules and 7 weeks for proteins, and over a 25-cm microcosm transport would take 1.5 and 100 years, respectively. In practice, macromolecules are unlikely to have to move

across the whole colony diameter, because transcription, translation, and localization in the case of proteins, or synthesis, packaging, and vesicle delivery in the case of wall components, are spatially localized on a much shorter length scale. Nevertheless, there is some evidence for long-distance protein translocation during fruiting in *Agaricus* ([58]).

In comparison with diffusive movement, motor-driven organelle transport can provide constant velocity transport in both directions over medium-length scales (millimeters to centimeters) both for the cargo transported, and also the bulk cytoplasm that becomes entrained ([40]). Fungi have some of the fastest microtubule motors known (1 to 4 μm s^{-1}) ([59]), while myosin V in yeast transports secretory vesicles at ~3 μm s^{-1} ([44], [60]). The maximum speed at which motors can move also places an upper bound on the velocity that can be achieved by motor-driven movement to approximately 4 μm s^{-1} (14.4 mm h^{-1}) ([61]). Actin-myosin-based cytoplasmic streaming in other systems, such as pollen tubes, can reach higher velocities, typically 40 to 60 μm s^{-1}, and reaching 100 μm s^{-1} with myosin XI in characean algae ([62]), but such high-speed motors do not seem to operate in fungi. The energetic costs of motor-driven movement would be expected to scale with the length of the transport pathway, particularly the cost of assembling the microfilament and/or microtubule tracks, the size of vesicles or organelles transported, the speed of movement, and the cytoplasmic viscosity ([62]). There are no quantitative estimates in fungi to our knowledge, but it is likely that the energetic costs are excessive, particularly in comparison with mass flow (see below). Nevertheless, this rate of movement may well be sufficient for species that do not forage far beyond their food resource, termed resource-restricted or non-translocators ([57], [63]), or for mycorrhizal fungi that have access to an abundant and consistent supply of carbon/energy from the host plant.

In addition to motor-driven transport, passive movement of solutes and organelles, such as vacuoles and nuclei toward the tip, can occur through mass flow of cytoplasm arising from a combination of expansion of the apical cell wall to create new volume, and subapical uptake of water and solutes ([32], [33], [64]–[68]), termed growth-induced mass flow (see [Fig. 1B], [2B], and [3]) ([33]). Quantitative microscopic measurements have been made on *Neurospora* hyphae, which have a relatively large diameter and grow at a maximum rate of 1 μm s^{-1} equivalent to 3.6 mm h^{-1} ([69]), thus capturing the fastest local transport events required for tip growth in any species. Injection of oil droplets, which cannot interact

directly with motors and the cytoskeletal system, provides direct evidence for growth-induced mass flow, as the rate of movement (about 5 μm s^{-1}) exceeds the rate of tip extension (0.2 to 0.5 μm s^{-1}) in these experiments ([66](66)). The actual velocity expected for mass flow depends on the number of downstream tips ([Fig. 2B](Fig. 2B); see "The impact of branching on transport" below). Likewise, nuclei, vacuoles, and mitochondria in apical compartments all migrate toward the growing tips at the same or greater rate than the tips extend ([64](64), [66–68](66)). Such movement would be consistent with mass flow driven by the continuous subapical water influx required to sustain volume increases at the tip during growth.

The time (t_A) taken for solutes or organelles to advect a distance l at velocity v is l/v, while the relative importance of advection compared with diffusion is given by the Péclet number, $t_A/t_D = vl/D_j$ ([62](62)). Advection dominates if this ratio is greater than 1, while diffusion dominates if this ratio is less than 1. Thus, the Péclet number for the apical compartment of *Neurospora* growing at 1 μm s^{-1} is approximately 0.3 for solutes and 20 for proteins. An alternative measure considers the length scale for localization of macromolecules, such as proteins and mRNA, depending on diffusion, advection, and their lifetime (τ) before degradation ([65](65)). Thus, localization scales as $\sqrt{D_j\tau}$ if diffusion and degradation dominate, $v\tau$ if flow and degradation dominate. The ratio $C = \sqrt{D_j/v^2\tau}$ of these two distances is a dimensionless number. If $C > 1$, then most transport occurs by diffusion, and if $C < 1$, then most transport is by flow ([65](65)).

Water Permeability and Water Uptake

The extent to which longitudinal mass flow occurs is critically dependent on precisely where water influx occurs in the colony. In principle, water could be taken up anywhere along the hyphae, but the actual site of uptake has profound implications for the magnitude and direction of internal mass flows. A second critical observation is that regardless of intrahyphal concentration gradients and turgor pressure resulting from solute accumulation, mass flow only takes place when water is able to exit the translocation pathway. A range of possible routes exists through either localized exudation ([70–73](70)), hydraulic redistribution to soil with lower water potential ([74](74)), evaporation during fruit body formation (e.g., *Phycomyces* sporangia) ([75](75)), coupling to the plant evapotranspiration stream in mycorrhizas ([76](76)), or by moving into a region of new growth ([33](33), [66](66)).

Fungi have a particular challenge to maintain a balanced water economy to allow water uptake for growth, while preventing excess evaporation from their extensive surface area. Equally, controlled evaporation may drive solute movement into aerial hyphae ([75](75)) and evaporative cooling may be required to aid spore dispersal by establishing convection currents ([77](77)), or through formation of "Buller's drop" by condensation ([78](78)). The plasma membrane provides some impedance to water movement, with permeability dependent on the lipid composition and temperature ([79](79)). Thus the osmotic permeability (P_f) of the plasma membrane in yeast mutants lacking aquaporins (AQPs) increases from 0.34 μm s^{-1} at 7°C to 2 μm s^{-1} at 23°C ([80](80)), equivalent to a plasma membrane water hydraulic conductivity coefficient ($L_w^{pm} = P_f \overline{V}_w/RT$) of ~2.5 to 15 × 10^{-15} m s^{-1} Pa^{-1}. It is worth noting that these values are 1 to 2 orders of magnitude lower than plant and mammalian cell membranes at the same temperature. Indeed, the presence of ergosterol in fungi, rather than cholesterol in other organisms, may be linked to greater resistance to desiccation ([81](81), [82](82)).

The presence of AQPs ([Fig. 1B](Fig. 1B)) also significantly increases water permeability in parallel to the lipid bilayer. For example, overexpression of AQPs in yeast increased P_f by 9-fold at 7°C. Likewise, expression of AQPs from the filamentous mycorrhizal fungus *Laccaria bicolor* in *Xenopus* oocytes increased the membrane permeability to up to 147 μm s^{-1} ([83](83)). Whereas the precise role of AQPs in water uptake has not been resolved, AQPs do appear to be critical in hydraulic coupling during fruiting and between mycorrhizal fungi and the host plant ([84–86](84)).

In both plant and animal systems there is also evidence for movement of water against the free energy gradient by chloride/cation cotransporters (CCC) ([87](87), [88](88)). CCC sequences are present in fungal genomes, but their role in fungal water economy has not been investigated to date. Nevertheless, this presents the interesting possibility that the low intrinsic plasma membrane water permeability in fungi, particularly at temperatures typically encountered in soils, might allow much greater regulated spatial control of the water economy through the localization and activation of aquaporins and CCC water pumps.

Hydrophobins and Control of Water Loss

To restrict water loss, many mycelia produce small (15 kDa) secreted cysteine-rich hydrophobin proteins that self-assemble to form a rodlet layer, particularly on aerial hyphae ([Fig. 1B](Fig. 1B) and [2A](2A)), and increase the hydrophobicity of the surface, thus restricting water movement ([89–91](89)). One benefit of using hydrophobins

A Branching, tropisms and fusion (anastomosis)

lateral branching

apical branching

aerial branching and hydrophobin coating

negative autotropism and hyphal avoidance

positive autotropism and anastomosis

100 μm

B Impact of branching and water uptake on flow velocity

$2^n v$

v v v v v v v v

All water uptake distal from tips – velocity scales as $2^n v$, where paths between hyphae and the tips pass $n+1$ branch points, and there are 2^n 'downstream' tips

v v v v v v v v v v v v v

water uptake even across mycelium – constant velocity in all hyphae

v v v v v v v v v v v v v v

water uptake only at tips – no flow in the rest of the mycelium

C Formation of multi-hyphal aggregates

Formation of tendril hyphae

tendril hyphae

0.5 mm

Loose strand formation

tendril hyphae

0.5 mm

Cord formation and vessel differentiation

fibre hyphae
tendril hyphae
vessel hyphae

0.5 mm

Multi-hyphal rhizomorph formation

rind
cortex
medulla
lacuna

2 mm

apical cap

D Long-distance translocation in multi-hyphal aggregates

Cytoplasmic streaming allowing both acropetal and basipetal movement of nutrients

v v v v v v v v

net acropetal mass flow in vessel hyphae in response to growth

to reduce evaporation is that their intrinsic organization varies with water availability, with no additional sensing or control other than their synthesis and secretion, allowing them to function autonomously outside the cell. Nevertheless, hydrophobins represent an expensive investment of scarce nitrogen resources, particularly as the cost of forming a functional barrier scales with the surface area of the hyphae covered. Thus, in more mature systems and multihyphal aggregates, hyphal walls tend to be impregnated with other compounds, such as melanin and phenolics, to reduce water evaporation and act as protection against damage and fungivores (92). Species vary in the extent of hyphal hydrophobicity, and this characteristic has been used to group mycorrhizal species as hydrophobic or hydrophilic (73).

In addition to chemical impregnation, there are biophysical constraints on water evaporation through the wall interstices depending on the diameter of pores in the cell walls generating a matric potential. There are few measurements of pore size in fungi, but in the water mould *Achlya* a value of 2 nm was determined experimentally (93). If terrestrial fungi have similar values, this would restrict evaporation, even at low external relative humidity, depending on the radius of the pores and wettability of the walls (79). While the role of matric potentials is well understood for the soil-plant-atmosphere continuum (79), we are only at the beginning of understanding water fluxes through the more complex soil-mycorrhiza-plant-atmosphere or soil-saprotroph-atmosphere systems (76, 94).

Insulating the hyphal wall leads to secondary problems on how the fungus can then sense the external chemical environment, how enzymes needed to decompose organic resources can be delivered, and how the products are then absorbed. Interestingly, there is evidence that enzyme delivery may be mediated by unconventional secretion through extracellular vesicles (EVs, exosomes), possibly derived from multivesicular bodies, that cross the wall (Fig. 1A) by an unknown mechanism (43, 95).

The Impact of Septation on Transport

In Dikarya, after a period of growth, the apical cell divides to establish a series of septal compartments that retain cytoplasmic continuity through the septal pores (Fig. 1C). Septa exhibit a variety of pore structures from narrow plasmodesmatal connections or simple uniperforate pores, to pores with associated Woronin bodies or other pore-occluding structures in the Ascomycota, and the more complex septal pore caps in the Basidiomycota (Fig. 1C) (96). The pore size ranges from 10 to 70 nm in the case of plasmodesmata and from 50 to 500 nm for most other pore types but is often partially occluded by electron-dense material (6, 96). Septal pores allow the passage of nutrients, macromolecules, and organelles between septal compartments. In some species, nuclei can also migrate through the septal pore (67, 69), while in the basidiomycetes, nuclear movement in heterokaryons is strictly controlled through the formation of clamp connections adjacent to the septum. The pore may be blocked reversibly or irreversibly by Woronin bodies (WBs) and septal pore associated (SPA) proteins in ascomycetes, or the septal pore cap (SPC) and its various elaborations in basidiomycetes (6, 97). Interestingly, the precise positioning and tethering of WBs have recently diverged in the Pezizomycotina, with more distal anchorage in rapidly growing species such as *Neurospora* (Fig. 1C), regarded as an adaptation to prevent accidental pore occlusion as high flow velocities sweep

FIGURE 2 Mycelial network formation: branching, fusion, and multihyphal aggregate formation. **(A)** Hyphae may branch subapically or by tip splitting to explore the substrate or to form aerial hyphae that are often insulated by hydrophobins. At the colony margin, tips avoid each other, while secondary branch hyphae in the colony interior can show positive autotropism and fuse by anastomosis. **(B)** The velocity of mass flow within the network depends critically on the site of water uptake for growth. If all water uptake is distal from the tips, the velocity scales in proportion to the number of downstream tips. If uptake is equal everywhere, the flow rate is constant at the speed of hyphal extension, while if uptake is solely at the tips, there is no long-distance movement. Based on references 32 and 33. **(C)** Schematic representation of the formation of strands, cords, and rhizomorphs, showing progressive differentiation of vessel hyphae as potential conduits for long-distance transport. Scale bars are approximate. Based on references 127, 129, 134, 228, and 265. **(D)** Schematic representation of how circulating fluid flows might operate within a hyphal cord. Acropetal mass flows would take place in the vessel hyphae in response to growth, evaporation, or exudation at the tips, while basipetal flows take place simultaneously through cytoplasmic hyphae by cytoplasmic streaming. Redrawn from reference 17 with permission.
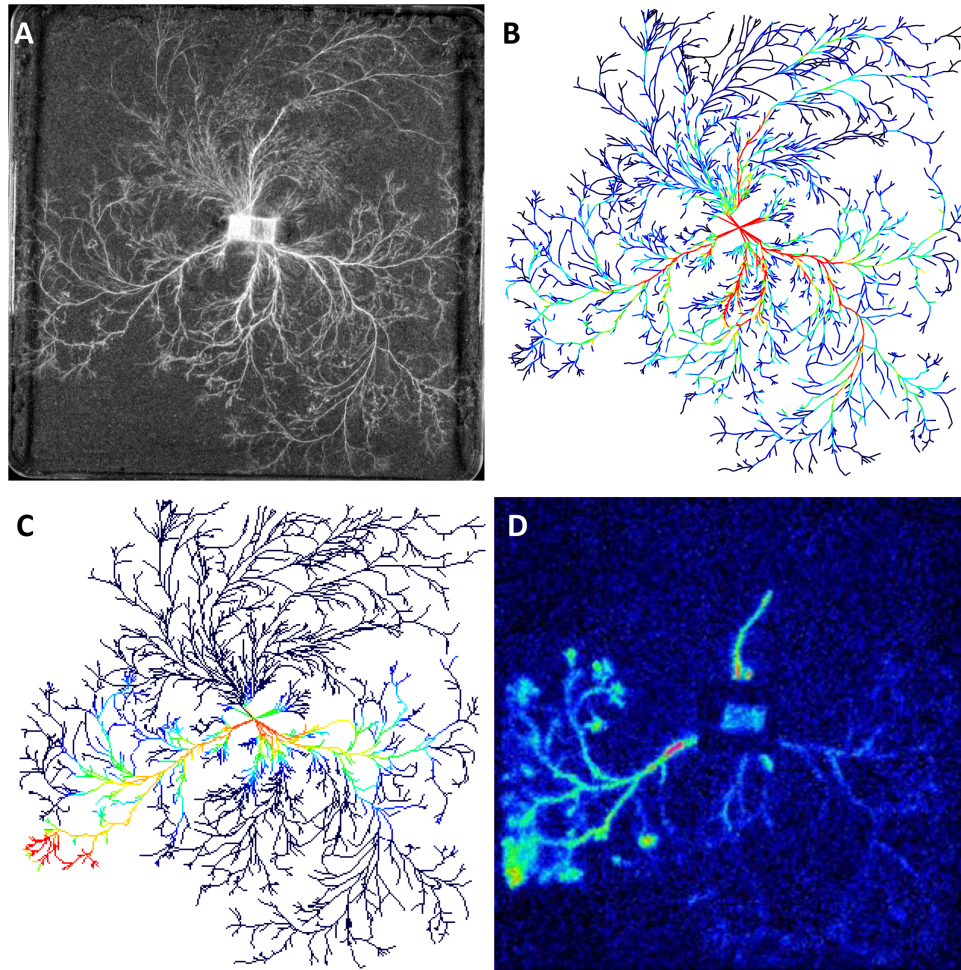
FIGURE 3 Growth-induced mass flows explain long-distance nutrient movement in *Phanerochaete velutina*. **(A)** Structure of the mycelial network after 21 days growing from a wood resource across compressed black sand. **(B)** The network architecture is extracted using intensity-independent, phase-congruency tensors and watershed segmentation from experimental time series. The output is a set of weighted adjacency matrices of the length, width, and volume of each cord. In this image, the cord width is pseudo-color coded from 50 μm (blue) to 500 μm (red). **(C)** The network structure and growth are input into a biophysical advection/diffusion/delivery (ADD) model, using growth-induced mass flow to predict the pattern of resource translocation. The predicted amount of radiolabel is color coded on a rainbow scale from blue (zero) to red (maximum). **(D)** The actual pattern of nutrient movement is then determined experimentally by using the nonmetabolized amino acid analogue ^{14}C-amino isobutyrate (^{14}C-AIB) and photon-counting scintillation imaging (PCSI). The amount of ^{14}C-AIB is color coded on a rainbow scale from blue (low) to red (high). The ADD model of growth-induced mass flow predicts the distribution of radiotracer in a complex network of fungal cords with a Pearson correlation coefficient 0.56. From Heaton et al. ([32](#)) with permission.

the WBs into the pore ([98](#)). While pore occlusion has a role in preventing loss of cytoplasmic contents after damage ([6](#)), there is increasing evidence that pore closure ([99](#)) or opening ([100](#)) can occur as part of a developmental sequence, and closure may be reversible depending on environmental conditions ([101](#)).

Even when open, the septal pore places an interesting constriction on fluid flow between septal compartments ([Fig. 1D](#)). The velocity of flow through septal pores (v_p) increases in proportion to the relative area of the pore to the cross-sectional area of the hypha (r_h^2/r_p^2), with experimentally measured velocities in ex-

cess of 200 μm s^{-1} in *Neurospora* ([69](#)), sufficient to restrict backward diffusion against the flow ([65](#)). Various organelles also accumulate in local eddies adjacent to the septa and, in the case of nuclei, appear to alter their protein complement as a result ([69](#)). Indeed, accumulation of secretory vesicles at septa may also be part of the trigger initiating branch formation ([102](#), [103](#)).

Fluid flows induce wall shear stresses, and in the case of laminar flow, the wall shear stress τ produced can be estimated using the formula τ = 4ηv/r, where η is the dynamic viscosity of the fluid, v is the mean velocity of fluid flow, and r is the radius of the vessel ([104](#)). In the typical case where the fungal cytoplasm has dynamic viscosity of 2 g s^{-1} m^{-1} and the hypha has a radius of 6 μm, the wall sheer stress is τ = v × 10^{-3}, where τ is measured in Pascals and v is measured in μm s^{-1}. By way of comparison, the wall shear stresses in mammalian arterial systems are in the range of 0.2 to 2 Pa, and it is known that stresses of that scale induce changes in gene expression ([105](#)). Hence, it is plausible that a 6-μm-radius hypha could detect and respond to internal velocities of the order of 1 mm s^{-1}, but along the length of most hyphae the wall shear stress will be negligible. However, because the mean velocity of fluid flow is inversely proportional to cross-sectional area, and wall shear stress is proportional to the velocity gradient at the wall, wall shear stress at the septal pore will be approximately r_h^3/r_p^3 greater than the wall shear stress elsewhere (where r_h and r_p are the radii of the hyphae and pore, respectively). This means that even the modest flows that have been measured in fungi can be expected to produce physiologically significant mechanical forces at the septal pore. Indeed, the scale of those forces can be estimated by measuring the elasticity of the cell wall and the amount of deflection that occurs during transient pore plugging, and in *Neurospora crassa* it has been calculated that the deflection-associated pressure difference is as large as 2 bar ([69](#)). Also note that the above equations somewhat underestimate wall shear stress, because the velocity profile deviates from the parabolic profile expected from Poiseuille flow due to the high density of organelles moving within the fluid ([68](#)). This analysis suggests that septal dissolution, branching, and other aspects of hyphal development may be directly influenced by the relative scale of flows within the hyphae ([33](#)), because the mechanical forces are large enough to degrade septa ([69](#)), and it is also plausible that fluid flows could be detected by proteins located at the septal pore, leading to flow-dependent changes in the pattern of gene expression.

Modeling Tip Growth and Branching

The number of growing tips at the colony margin increases by apical or subapical branching and daughter hyphae typically show avoidance behavior (negative autotropism, [Fig. 2A](#)) regulated by the Cdc42 signaling pathway ([7](#), [106](#)) to increase exploration of the substrate ([Fig. 2A](#)). The fact that fungi grow by apical extension, although intercalary growth has been observed ([107](#), [108](#)), implies that there is a fundamental relationship between the overall colony growth rate and the branching rate. This relationship can be clarified by letting A denote the mean cross-sectional area of individual hyphae, N(t) denotes the number of hyphal tips at time t, g(t) denotes the specific growth rate of the colony (that is, the rate of change of volume per unit volume of fungus), and v(t) denotes the mean velocity of hyphal tips. If all growth is due to apical extension, it follows that the mean volumetric growth rate of an individual tip is Av(t), and the total volumetric rate of growth $\frac{dV}{dt} = V(t)g(t) = AN(t)v(t)$. It follows that:

$$N(t) = \frac{V(t)g(t)}{Av(t)} \qquad (1)$$

When the specific growth rate g and the mean velocity of hyphal tips v are constant, the rate of change of the number of tips is:

$$\frac{dN}{dt} = \frac{\frac{dV}{dt}g}{Av} \qquad (2)$$

Equations 1 and 2 imply that when the specific growth rate g and velocity of hyphal tips v are constant, we have:

$$\frac{\frac{dN}{dT}}{N} = \frac{\frac{dV}{dt}}{V} = g \qquad (3)$$

Note that the number of tips is increased by each branching event and decreased by each fusion (anastomosis) event, so we cannot conclude that the branching rate is simply equal to the specific growth rate g. Nevertheless, it is reasonable to assume that the branching rate is only slightly larger than the specific growth rate g, which is a claim that has empirical support ([102](#), [109](#)). If the branching rate is equal to the specific growth rate, there must be a constant relationship between the volume of hyphae and the number of hyphal tips. In 1959, Plomley ([110](#)) observed that exponential colony growth requires continual branching, and he speculated that

when a species is growing exponentially, there is a constant volume of fungus per hyphal tip termed the "hyphal growth unit." This is the key concept behind the mathematical models of hyphal growth developed in the 1970s ([102](#), [109](#), [111](#)–[113](#)), which recapitulate the experimental observation that the velocity of hyphal tips is initially proportional to the volume per hyphal tip (e.g., reference [69](#)). Thus, the rate of germ tube extension is initially exponential as the increasing volume of cytoplasm provides more vesicles per tip. As the colony grows, the rate of vesicle delivery reaches a maximum and the mean tip velocity approaches a constant as a result, obtaining a value for the hyphal growth unit that is characteristic of the species in the given environment and manifest at a colony level as the width of the peripheral growth zone ([111](#)).

Linking Growth and Branching to Nutrient Status

Like all organisms, fungi require a source of energy and nutrients to sustain growth, and so the specific growth rate and branching rate of fungi must be smaller for fungi that grow on substrates that are recalcitrant or nutrient poor ([114](#), [115](#)). This kind of energetic constraint on fungal growth has implications for the optimal allocation of resources toward vegetative growth, the production of digestive enzymes, and the production of spores ([31](#)). Any successful model of hyphal growth must recapitulate the fact that nutrient availability enables growth, and rapid growth is associated with rapid branching. However, because of the difficulty of observing fungal growth and a lack of understanding of the control of branching, there are few statistics concerning the location of branching events in a growing fungus ([116](#)). On a macro scale, models of the branching process generally make the reasonable assumption that branching is more likely to occur in regions with a higher density of tip-growth vesicles ([29](#), [102](#)), which may occur when vesicles are too far downstream of the apex to be able to contribute to growth of the apex itself and are therefore diverted to form a new growing tip ([102](#), [117](#)). On a micro scale, it has been suggested that branching is associated with septa because vesicles may accumulate around septal pores ([102](#), [103](#), [109](#), [117](#)). However, it is not known whether, all else being equal, younger hyphae are more likely to branch, or whether hyphae that carry relatively large mass flows are more likely to branch.

Hyphae can also form in older parts of the colony by secondary or lateral branching, to an extent dependent on the species, the medium of growth, and other environmental factors ([8](#), [118](#), [119](#)), but there are significant differences in the cellular mechanisms involved in apical and secondary tip formation ([120](#)). Watters et al. ([121](#)) demonstrated that the distribution of distances between adjacent branch points is independent of tip extension rate in *N. crassa* at a range of temperatures. However, following a sudden increase in temperature (and metabolic rate), there is a transient increase in branching rate, while, following a sudden decrease in temperature, hyphae produce an unusually long branch interval ([122](#)). These observations are consistent with the following four assumptions:

1. The rate of tip extension is proportional to the rate of vesicle deposition.
2. The rate of branching is proportional to the number of vesicles in the colony.
3. The rate of vesicle production is proportional to the metabolic rate of the colony, and this rate changes relatively rapidly when the metabolic rate is altered by changing temperature.
4. The rate of vesicle deposition at the tips is proportional to the metabolic rate of the colony, and this rate changes relatively slowly when the metabolic rate is altered by changing temperature.

If these plausible assumptions are correct, a sudden increase in temperature will increase the rate of vesicle production more quickly than it increases the rate of vesicle deposition, creating a transient increase in the density of vesicles within the colony, which produces an increase in the branching rate. Also note that, if the velocity of hyphal tips and the specific growth rate of a fungus remain fairly constant, the diameter of the fungal colonies will grow in a linear manner, while the volume of that same colony will grow exponentially. This implies that the density of the fungal growth will increase, although at some point population effects will start to inhibit growth because, in the dense core of the colony, the concentration of inhibitory waste products will be relatively high and there will be relatively few nutrients or space to enable further growth.

The Impact of Branching on Transport

Branching reduces the radial distance that can be supplied by diffusion alone ([53](#)), but has no effect on the velocity of motor-driven transport, although the total flux is halved at each branch point. The extent to which branching affects organelle and resource distribution by mass flow depends on the site of water uptake ([16](#), [32](#), [33](#)). At one extreme, if water uptake only occurs at the

initial inoculum, volumetric mass flow scales with the number of downstream tips that are growing (Fig. 2B). If water uptake takes place equally across the network and the cross-sectional area is constant, the velocity in each hypha matches the rate of growth, while, if all uptake takes place at the tips, there is no mass flow in the rest of the colony. In wild-type or the *so* mutant of *Neurospora*, which is unable to fuse and thus only grows as a branching tree (123), nuclear movement occurs predominantly by mass flow, and the rate scales with the number of downstream tips, reaching values of 5 to 20 µm s^{-1} (67, 69), consistent with water uptake at the center of the colony or germinating conidium. Thus, in *Neurospora*, even though water is freely available in the substrate, uptake is highly spatially regulated to ensure high rates of longitudinal flow through the colony.

The Impact of Hyphal Fusion on Transport

Fusion may take place early in colony formation *via* conidial anastomosis tubes (CATs) that potentially link multiple conidia into a supracellular network (11–13). Secondary branch hyphae also develop in more mature regions when daughter hyphae typically show positive autotropism and fuse with neighbors to create a microhydraulic network with loops (7, 9, 11–13, 49). Fusion appears to be required for high rates of long-distance nutrient translocation, as the *so* mutant in *Neurospora* shows reduced radiolabeled amino acid movement (124). Nevertheless, loops are probably more critical in providing multiple pathways to improve network resilience and to allow rapid reallocation of resources in response to local demands. For example, lateral movement of radiotracers at the colony margin (125) probably occurs as a result of anastomosis.

Hyphal Differentiation and the Formation of Multihyphal Aggregates

In many species, there is some differentiation into leader or trunk hyphae and aerial hyphae at the colony margin (Fig. 2C). However, formation of linear hyphal aggregates, such as cords and rhizomorphs, only occurs to a lesser extent on agar, so there is comparatively little information on the development and internal structure of these organs from laboratory studies.

Cords form behind the front of apically extending hyphae, with the degree of hyphal aggregation within the growing front varying between species (126, 127). Close to the growing front, both large- and smaller-diameter hyphae are normally present with many branches and anastomoses interconnecting both hyphal types. In corded systems, large-diameter hyphae are

initially cytoplasmic, with progressive cellular disorganization and appearance of empty vessel hyphae with distance from the front (17, 128). In *Serpula lacrymans* narrow tendril hyphae emerge from the clamp connections and then branch and grow both acropetally and basipetally around neighboring hyphae (129). In more developed cords, cross sections at the light or EM level show further differentiation of thick-walled fiber hyphae and vessel hyphae, with diameters of approximately 10 to 15 µm, that are likely to improve flow (Fig. 2C). During early development, movement of radiotracers and fluorescent dyes appears to be restricted to particular routes that probably correspond to developing cords (125, 130–132), although tracking the internal connectivity has been rarely attempted. The size of the vessel hyphae can have an impact on the flow rate, which scales as r^4, but flow will be more critically dependent on the size of the septal pores and the extent of septal dissolution associated with cord formation (126, 127). Nevertheless, ectomycorrhizal cords of *Paxillus* have swollen clamp connections at the nodes that provide continuity with the branches, but only limited septal dissolution in the vessel hyphae (133).

Rhizomorphs are more highly differentiated root-like structures that extend from a meristematic-like region at the tip (Fig. 2C). They consist of a central lacuna surrounded by an inner medulla with large thin-walled vessel hyphae that form high-conductivity channels, an outer medulla containing loosely packed hyphae that are only about 2 µm wide, and a thick melanized, hydrophobic rind that insulates them from the environment. The longitudinal hydraulic conductivity ($L_w^{\parallel}$) through the cords varies from 1.5 to 3×10^2 cm^2 bar^{-1} s^{-1} (134). The hydraulic conductivity perpendicular to the hyphal axis ($L_w^{\perp}$) for such cords has not been measured, but is likely to be low.

Pressure-Driven Mass Flow on a Macroscopic Scale

The velocity of water movement in corded systems or rhizomorphs is vastly in excess of values that could be achieved by motor-driven movement, and initially led to the idea of pressure-driven mass flow as the major transport mechanism in foraging fungi (15, 135). Thus, estimates of water transport in *Suillus bovinus* were 27 cm h^{-1} (136), while measurements in *S. lacrymans* have a mean value of 148 cm h^{-1} (70). Likewise, a range of different solutes is transported in *Armillaria* at velocities in excess of 20 mm h^{-1} (137), in *Serpula* ranging from 10 to 50 mm h^{-1} (138) to 20 to 30 cm h^{-1} (135, 139), or 20 to 100 mm h^{-1} in *P. velutina* depending on

the extent of cord formation (32, 33, 131, 132; Fricker et al., unpublished data). Similarly, even movement of larger organelles, such as nuclei, by mass flow can reach velocities of up to 4 mm h^{-1}, although there is wide variation in velocity between different hyphae in the network (67).

The magnitude of growth-induced mass flows has been empirically determined by measurements of network growth at the level of individual cords (Fig. 3A and B) (33), and input into an advection-diffusion-delivery (ADD) model to predict the pattern of resource translocation (Fig. 3C) (32). The actual pattern of nutrient movement was then determined experimentally using non-metabolized radiotracers and photon-counting scintillation imaging (PCSI; Fig. 3D). The ADD model of growth-induced mass flow is surprisingly effective at predicting the distribution of the amino acid analogue ^{14}C-amino isobutyrate (^{14}C-AIB) in a complex network of fungal cords (compare Fig. 3C with Fig. 3D). This is remarkable considering the conceptual simplicity of the biophysical model, and that there is essentially only one free parameter, the fraction of the cord that carries nutrient flow.

The magnitude and direction of mass flows can be altered by experimental manipulation of the external water potential, but it is also clear that, under natural conditions, the external water potential can have an impact on transport through the network. Thus, substantial water flow (18 cm h^{-1}) can be driven by hydraulic redistribution from moist to dry soil (74), or through hydraulic coupling to the host plant (27 cm h^{-1}) in the case of mycorrhizas (136, 140).

Biomass Recycling

As some hyphae expand and mature, other regions of the mycelium regress and their contents are recycled. In particular, there is extensive remodeling of redundant parts of the mycelium in larger mycelia grown from woody resources (see "Colony dynamics and behavior" below), presumably to redeploy resources to the growing margin to forage more efficiently in highly heterogeneous environments (14, 31, 56, 141, 142). Interestingly, in other systems, such as blood vascular networks and slime molds, recycling and network remodeling occur in response to flow rate (143), and there is evidence that a similar relationship between high flow and cord thickening, versus low flow and cord thinning, holds for fungi (33, 144).

At a molecular level, recycling probably involves autophagy and controlled apoptotic-like mechanisms, rather than necrosis (145, 146). Nevertheless, how decisions are made to trigger autophagy in particular hyphae are not clear, nor is it clear how the cytoplasm and wall materials are broken down and transferred to the growing front.

Bidirectional Movement and Oscillations

There is plenty of evidence for nutrient translocation from resources to the growing margin where they are needed for growth. However, in several systems, radiotracer measurements indicate that nutrients can move both acropetally and basipetally in the same colony or following colony fusion (125, 137, 138, 147–152). Bidirectional movement is likely to be critical to achieve mixing of spatially distributed food resources between constantly changing sources and sinks and therefore promote maximum colony growth in a heterogeneous environment, and may also contribute to colony-wide control of behavior (56). Over short length scales, diffusion and motor-driven transport may achieve transport at a sufficient rate, but responsive resource allocation in larger colonies requires mass flow. However, simultaneous bidirectional movement is difficult to explain based solely on pressure-driven mass flows, which would be expected to operate in one direction at a time, so models have invoked distinct pathways that involve acropetal mass flows in vessel hyphae and basipetal streaming in adjacent cytoplasmic hyphae (Fig. 2D) (17). In addition, some species, such as *P. velutina* (131, 132, 153), but not others, such as *S. lacrymans* (138) or *N. crassa* (124), show marked oscillations superimposed on the net transport. The origins of the oscillations are not known, but may represent a reciprocating transfer of material, rather than the continuous circulatory system shown in Fig. 2D. This is reminiscent, albeit at a much longer time scale, of the shuttle streaming in *Physarum polycephalum* that leads to efficient mixing within the plasmodium (154).

COLONY DYNAMICS AND BEHAVIOR

In discrete organic resources saprotrophic mycelial networks typically operate on a millimeter to centimeter scale, depending on the size of the resource and size of the genetic individuals. However, large individuals occupying extensive decay columns in tree trunks and branches operate over a larger scale. Furthermore, those fungi that are non-resource-unit-restricted extend from their main food base into the surrounding environment in search of new resources (Fig. 4 through 7), and often operate on the scale of meters. Thus, saprotrophic systems of mycelia cords and rhizomorphs cover
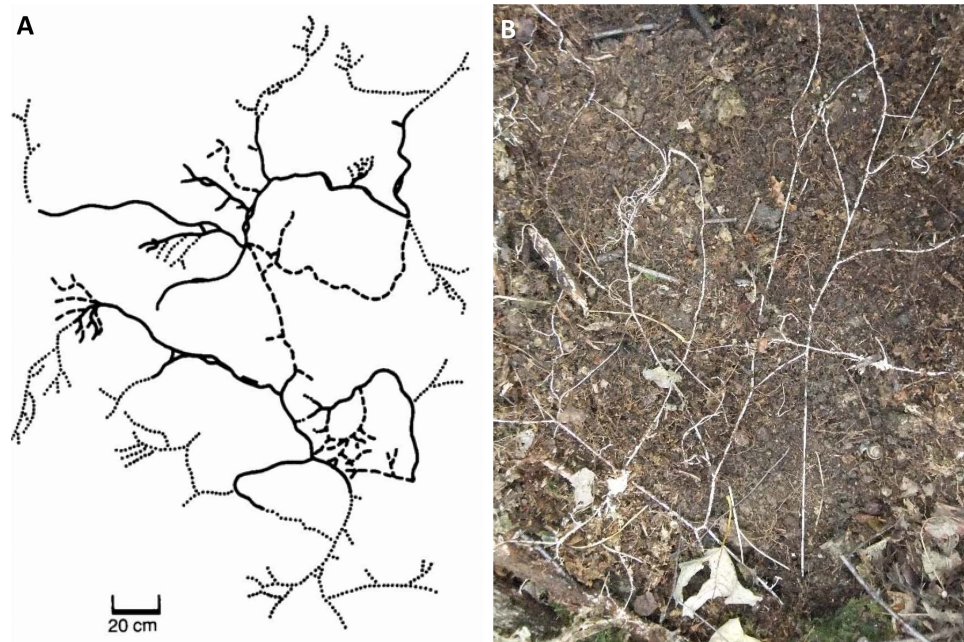
FIGURE 4 Mycelial networks in woodland. **(A)** Map of a mycelial cord network of *Phanerochaete velutina* revealed by carefully removing surface litter layer, recovering, and then re-revealing 13 months later. From Thompson and Rayner ([155]) with permission. **(B)** Network of *Megacollybia platyphylla* on the floor of a mixed deciduous woodland, following removal of surface litter.

several square meters to many hectares ([Fig. 4]) ([135], [155], [156], [157]). Currently, the largest recorded genet is of *Armillaria ostoyae* spanning 965 hectares, with a maximum separation of extending fronts of 3,810 m ([157]), although the extent of internal connectivity is unknown.

There is little information on mycelia networks within organic resources (see "Extension of network analysis to 3-D" below), except for the boundaries of territory occupied by individual mycelia, indicated by interaction zone lines ([36]). Likewise, little is known of the structure of networks of non-resource-unit-restricted fungi foraging in relatively homogeneous resources, e.g., fairy ring formers and colonizers of leaf litter patches ([36]). The latter are particularly interesting because they extend through the leaf litter layer as an ever-increasing annulus of mycelium, about 30 to 40 cm wide in the case of *Clitocybe nebularis*, differentiated into several distinct zones ([158]).

A wide variety of patterns of mycelial outgrowth from organic resources has evolved, ranging between slowly extending search fronts densely populated by hyphae, which are unlikely to miss new resources, e.g., *Hypholoma fasciculare*, to more rapidly extending but sparser systems, e.g., *P. velutina*, and at the furthest extreme *Armillaria* species. The slow-dense foragers are often considered short-range foragers, and have sometimes been termed "phalanx or phalangeal foragers" ([34], [35], [159]), by analogy with foraging of clonal plants that grow relatively slowly and have tight aggregated rosettes ([160]–[163]). The fast-effuse foraging, on the other hand, is often considered long-range foraging, and has been likened to "guerrilla" foraging of plants (clones of which have fast-growing branches that are loosely aggregated). Similar concepts have been developed for mycorrhizal networks that include short-range "contact exploration types" and "long-distance exploration types," where the mycelium is highly differentiated into strands ([164]). Other similar, but not identical, ideas have been put forward by plant ecologists, such as "clump" plants characterized by frequent branching at large angles and with short spacers, which exploit resources at a particular site, and "runners" with infrequent branching and long spacers, which explore more widely for resources ([165], [166]). Parallels have also been drawn between fungal and animal foraging ([163], [167]).

Perhaps the most dramatic alterations in mycelial network structure occur when new resources are discovered, either by a foraging mycelial front, or when resources land on an established system ([Fig. 5]). When mycelium encounters a new resource, parts of the network connecting the original with the new resource
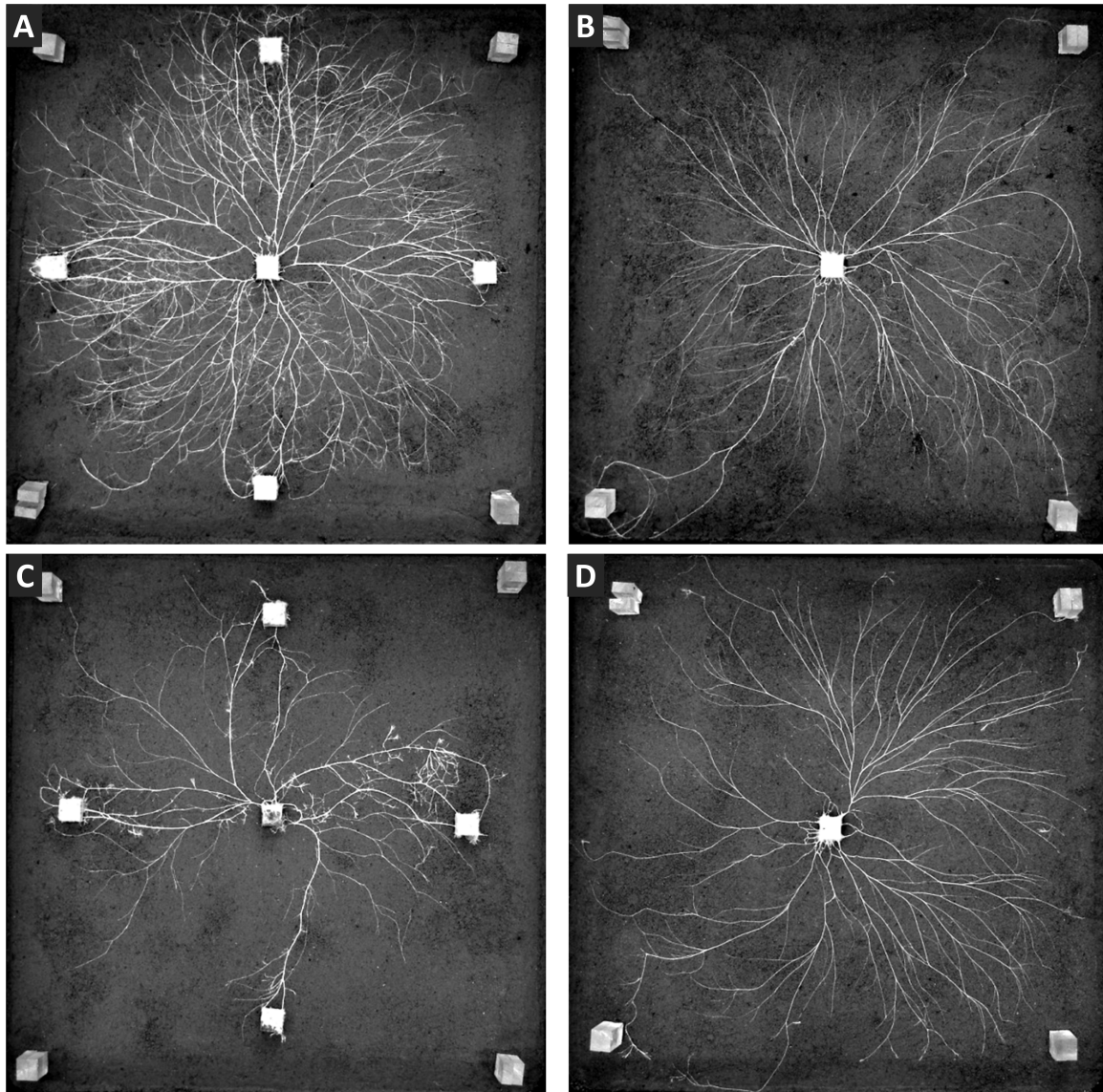
FIGURE 5 Effects of resource addition and grazing on mycelial networks. Mycelial cord systems (99 days old) of *Phanerochaete velutina* growing from centrally positioned beech wood inocula across the surface of compressed nonsterile soil in 50 × 50 cm trays. **(A)** With four additional beech wood blocks added behind the mycelial margin 36 days after central inoculation. **(B)** With no additional resources added. **(C)** As in A, but with 250 laboratory-reared collembola, *Folsomia candida*, added 49 days after the central inoculums. **(D)** As in C, but with no additional resources. From Wood et al. ([170](#)), with permission.

aggregate to form mycelial cords, while nonconnecting mycelium dies back ([168](#)). The rapidity and extent to which this occurs depends, among others, on the foraging strategy of the fungus, the relative size/quality of the original and new resources, and the presence/absence of invertebrate grazers ([34](#), [35](#), [169](#), [170](#)). Short-range foragers reallocate their biomass rapidly and extensively, with often only the connective cord and outward growth from the newly colonized resource remaining after a few months. In contrast, little reallocation of mycelial biomass occurs in long-range foragers unless the newly encountered resource is considerably more substantial than the original resource. The process is speeded up if grazing invertebrates are present; fine mycelium disappears more rapidly than if they are absent, leaving only larger mycelial cords ([Fig. 5](#)). These

processes occur repeatedly on the forest floor, producing large, open networks of cords interconnecting discrete organic resources ranging from small twigs to large tree trunks (Fig. 4). How the decision is made to strengthen or recycle a particular cord is not clear, nor is the mechanism that serves to retrieve useful breakdown products and redirect them to regions of new growth.

Interestingly, strands of *Pleurotus ostreatus* and rhizomorphs of *Armillaria gallica* (formerly *bulbosa*) both show spontaneous action potentials between 0.5 and 5 Hz, and the frequency increases in response to addition of nutrients (171, 172). Furthermore, the signal propagated across the colony at a speed of 0.5 mm s^{-1} over distances of a few centimeters when nutrients were added remotely. Similar potentials have been reported in a number of other species, and it has been proposed that they may play a role in coordinating growth and differentiation by preventing hyphae from undergoing apoptosis and strengthening cord formation (172).

QUANTITATIVE ANALYSIS OF NETWORK ARCHITECTURE

Constraining the Problem to 2-D

Our understanding of the coordinated growth and behavior of fungal networks has been limited by the immense practical difficulties associated with measuring organisms that exhibit indeterminate, highly plastic growth. Although fungi would normally grow as three-dimensional networks through opaque media such as soil, wood, plant, or animal tissue, most morphological studies have constrained growth to two spatial dimensions to simplify image collection and analysis. Furthermore, the substrate is usually limited to transparent media such as agar plates (e.g., 173), often overlaid with cellophane membranes (174, 175), or as dispersed mycelia in submerged cultures (176–178). There is a challenge to achieve both sufficient magnification to resolve individual hyphae and sufficient scale to map the entire network. Magnifications typically range from 10 to 100× using microscopes (179, 180), but photographic enlargers (174, 175, 181) or flatbed scanners can also be used (173). Colonies can also be grown on cellulose nitrate membranes on agar (182) or soil (183), and visualized following fixation, staining, and rendering the membrane translucent with immersion oil to enhance contrast (182). Alternatively, colonies grown on soil can be repeatedly sampled and growth quantified by using an immunoblotting technique (184).

Network organization is relatively easy to observe at the growing margin of the colony on transparent media. However, submarginal growth is denser and includes aerial hyphae, which makes it difficult to track individual hyphae and discern the pattern of branching and anastomosis. Thus, most network analysis is limited to a short period (<72 h) of surface growth over short distances (millimeters to centimeters) (e.g., 173), although confocal imaging can be used to analyze 3-D distribution of aerial and penetrative hyphae labeled with Congo Red (185, 186). More recently, confocal fluorescence imaging following wall labeling with calcofluor white has allowed quantitative measurements of early colony formation in 3-D over an extended period (17 days) and represents the first time the dynamics of critical parameters such as branching length and angle have been determined throughout a colony (116). At a more macroscopic scale (centimeters to meters), saprotrophic fungi have been studied the most because they are straightforward to culture from woody resources as a planar 2-D system on nonsterile compressed soil or sand that can be readily imaged (Fig. 4 through 7).

Fractal Measures and Hyphal Coverage

The simplest quantitative measure of colony behavior is surface area coverage from the number of pixels that make up a mycelial image. However, like many natural structures, mycelia are approximately fractal, and fractal geometry may be more appropriate to describe the systems (173, 187, 188). The fractal dimension quantifies the extent to which mycelia fill space relative to the size of the mycelial system. In two dimensions, e.g., the surface of soil, its value ranges between 1 (a line) and 2 (a filled surface). In three dimensions it could take an upper value of 3, although three-dimensional mycelial systems have rarely been investigated. Two types of fractal dimension have been used to provide different measurements of the branching/space filling of mycelia: the mass fractal dimension (D_M) and the surface (or border) fractal dimension (D_S, a subset of D_M), which only describes the edge of the mycelial system. Both are important because they allow a distinction to be made between systems where there are gaps inside (i.e., hyphae do not entirely fill the space), and those systems that have plane-filled interiors and are only fractal at their edges/borders.

Several methods are available for calculating fractal dimension, the most commonly used for mycelia in natural and seminatural (i.e., not agar) situations, e.g., mycelia growing across the surface of soil, is the box-counting technique (188). Effectively, a series of grids of square boxes of different sizes (i.e., different numbers of pixels in an image; 3 to 63 being appropriate for mycelia

in small [24 × 24 cm] soil microcosms) is overlaid onto an image of the mycelium. The number of boxes intersecting pixels of the mycelium is recorded. The box-count fractal dimension is given by D in equation 4:

$$N(s) \approx cs^{-D} \qquad (4)$$

where $N(s)$ is the total number of boxes having side length s that intersect the mycelium image; c is a constant. There are two types of boxes: interior boxes (i.e., those that contain only pixels of the mycelium) and border boxes (i.e., those that contain at least one mycelial pixel and contain or adjoin at least one non-mycelial, e.g., soil, pixel). So the total number of boxes, $N(s)$, is given by equation 5:

$$N(s) = N_{border}(s) + N_{interior}(s) \qquad (5)$$

Regression of the linear part of a plot of $\log N_{border}(s)$ against $\log s$ provides an estimate of D_S (equation 6):

$$\log N_{border(s)} = \log c - D_s \log s \qquad (6)$$

Likewise, regression of the linear part of a plot of $N_{interior}(s)$ against $\log s$ provides an estimate of D_M. D can be estimated for entire mycelia, or for distinct areas of local interest by using software such as FracLab for MatLab (https://project.inria.fr/fraclab/) or FracLac for ImageJ (189).

Fractal dimension and hyphal coverage per unit area vary considerably between species, during mycelial development, depending on abiotic conditions, and are altered by interspecific interactions with other organisms (188). D_M of mycelia in small (24 × 24 cm) microcosms of compressed soil (nonsterile, i.e., similar to the natural environment) ranges from 1, for the linear rhizomorphs of fungi such as *Armillaria* spp. and *Megacollybia platyphylla*, to close to 2, for the densely packed mycelia of *H. fasciculare* and *Stropharia caerulea* (Fig. 6). However, even for the latter two species, D_M decreases with time and increasing size of the system, with networks becoming sparser as mycelial cords form and interstitial hyphae die back. These mycelia with, at least, initially high D_M have lower D_S, indicating that they are surface/border fractal systems, i.e., only the edge of the system is fractal. Others have similar D_M and D_S, indicating that the whole system is fractal. Those fungi that are mass fractal tend to extend more rapidly than those that are border fractal, implying that there is a balance between space filling and extension rate. Trade-offs when deploying mycelial biomass in search of new resources,

and for other attributes such as resilience, are considered in more detail below.

Fractal geometry is affected by the quantity and quality of the resources available to the mycelium, including size of resource, number of resources, addition or encounter with new resources, and the nutrient status of soil through which the mycelium is growing (35, 187, 188). For example, D_{BM} and D_{BS} of *H. fasciculare*, *P. velutina*, and *Resinicium bicolor*, but not *S. caerulea*, increased with increasing inoculum size (from 0.5 to 4 cm^3). *S. caerulea* systems growing from well-decayed (84 days old) inocula took 10 days longer to achieve the same D_{BM} and D_{BS} values as when mycelia were growing from relatively undecayed (22 days old) inocula. D_{BM} and D_{BS} were often lower for mycelia growing across soils with relatively low phosphorous and nitrogen content, short-range foragers often being more responsive to nutrient addition than the longer-range foragers. Non-nutrient environment factors, including water potential, temperature, and pH, also sometimes affect D (188). For example, D_{BS} of *S. caerulea* decreased with increasing water potential (i.e., getting wetter) from –0.02 MPa to –0.002 MPa, whereas with *P. velutina* there was little effect. D_{BM} and D_{BS} of *P. velutina* were significantly less at 5°C than at 10 to 25°C for several weeks, although the effects on *S. caerulea* were variable. Interactions with other fungi can also dramatically influence mycelium characteristics including hyphal coverage and fractal dimension, which varies between combinations of species and alters locally reflecting attack or defensive responses (190).

Graph-Theoretic Network Representations

Fractal measures capture some aspects of network organization, but advances in image analysis now mean that an explicit representation of the network structure is possible. Early image analysis routines (reviewed by references 176 and 177) used simple gray-scale thresholding (116, 180) or Sobel or Canny edge detectors followed by image opening and hole filling (191) to segment the hyphae. The resultant binary image is typically thinned to a single-pixel-wide skeleton and can be converted to a graph representation, where each junction is classed as a node and the intervening segment as a link. These approaches have the advantage that they can be readily implemented in open-source software packages, such as ImageJ (e.g., 182, 192).

More recent approaches use additional ridge enhancement algorithms, adaptive thresholding, and pruning steps to aid segmentation (173, 193, 194). Most current algorithms for network extraction were origi-
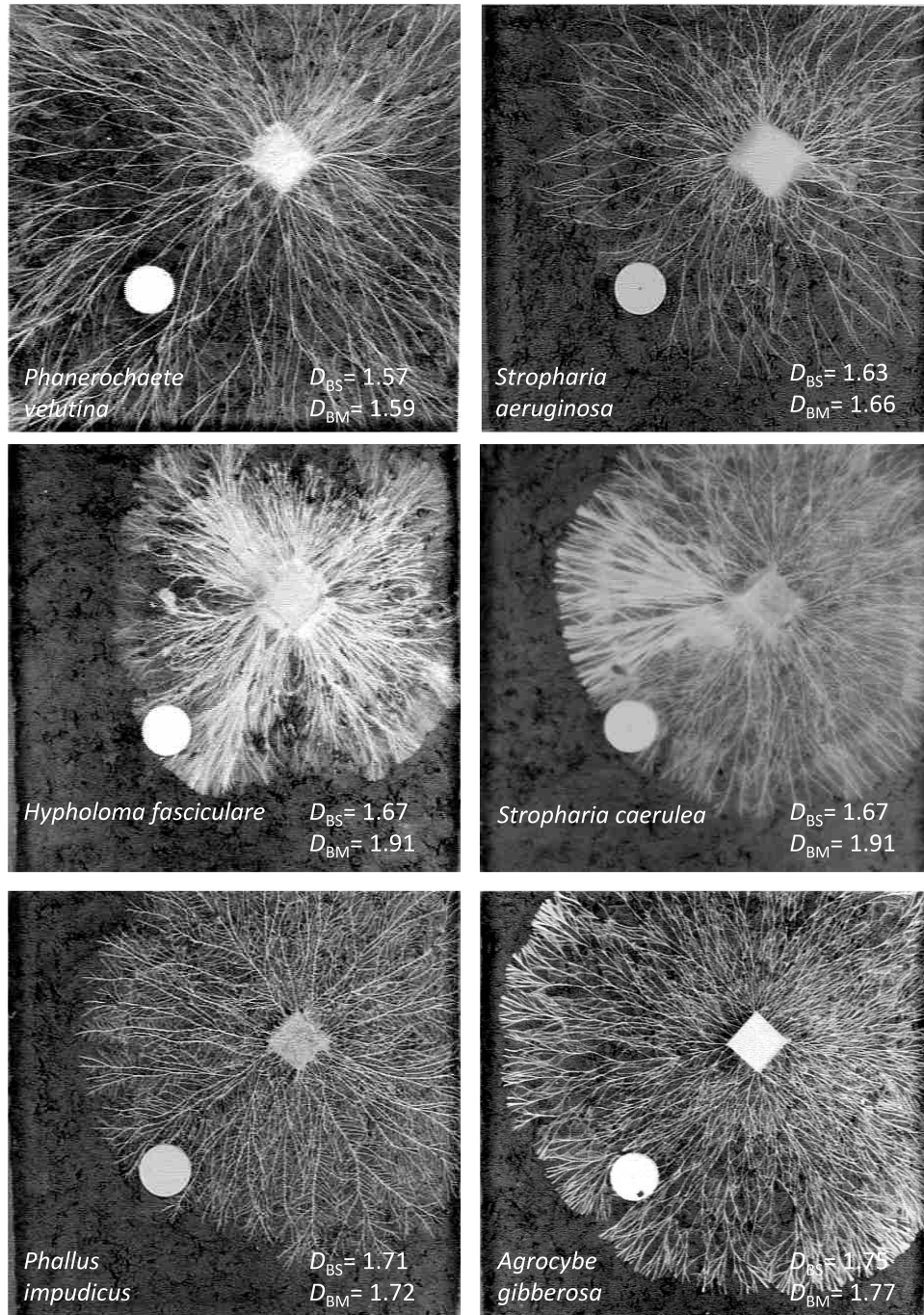
Phanerochaete velutina $D_{BS}= 1.57$ $D_{BM}= 1.59$

Stropharia aeruginosa $D_{BS}= 1.63$ $D_{BM}= 1.66$

Hypholoma fasciculare $D_{BS}= 1.67$ $D_{BM}= 1.91$

Stropharia caerulea $D_{BS}= 1.67$ $D_{BM}= 1.91$

Phallus impudicus $D_{BS}= 1.71$ $D_{BM}= 1.72$

Agrocybe gibberosa $D_{BS}= 1.75$ $D_{BM}= 1.77$

FIGURE 6 Species variation in fractal dimensions. Mycelia of six wood decay fungi extending, for 28 days, from centrally positioned beech wood inocula across the surface of compressed nonsterile soil in 24 x 24 cm trays. White circles are inert plastic discs. Note the different surface (D_{BS}) and mass (D_{BM}) fractal dimensions of the mycelia of different species. Photographs courtesy of Damian P. Donnelly. From reference 35 with permission.

nally developed for blood vascular systems or neurons, and typically involve enhancement of the "ridge" nature of the hypha or hyphal aggregate. The most common approaches use second-order derivatives of a Gaussian over a range of angles and scales (e.g., 195), although pattern-matching templates can also be used (196). Anisotropic kernels are more powerful because they emphasize the elongated shape of network segments and have recently been developed specifically to analyze mycelial networks (197). The maximum response of the filter provides information on the edge strength and its orientation, while additional measures, such as the anisotropy of the first three eigenvalues, give a measure of how strongly the edge corresponds to a (blood) vessel ("vesselness," 195). An alternative approach uses local phase congruency to give an intensity-independent approach to edge enhancement. This provides better segmentation for larger microcosms with cords, when the edges vary in intensity as well as scale and orientation (Fig. 7A and B), but at the expense of greater computational cost. The phase-congruency measure can also be combined with tensor-based measurements to give the phase-congruency equivalent of "vesselness" (193, 198). The enhancement step is followed by segmentation using non-maximal suppression and hysteresis thresholding (197), watershed segmentation, and edge pruning (193), or a reverse diffusion-based algorithm (196) to give a single-pixel-wide skeleton.

A complete description of the mycelial network also requires an assumption of the hyphal width (e.g., 173), or experimental estimation from the network image (32, 33, 144, 169, 175, 193). This is still a technically challenging area with a number of methods available that use slightly different assumptions. For example, a granulometry approach can be used whereby the intensity image is subject to a series of image openings (erosion followed by dilation) that successively remove structures as the size of the opening kernel exceeds the underlying object (193, 198). The intensity of each pixel initially decreases slowly as the kernel samples more of the object, but then reduces dramatically once the boundary of the object is reached, and the kernel only samples the background. The transition point for any pixel is determined from the maximum (negative) gradient of the granulometry curve. However, this approach constrains the radius to integer pixel values, and also suffers from digital approximation of small kernels to a true disk-shaped kernel. Thus, rather than extract a specific size threshold, the integrated intensity under the granulometry curve can be calculated to provide a more nuanced interrogation of the local image intensity

profile. The integrated intensity cannot be directly related to the physical width without additional assumptions about the relationship between intensity and sampled volume through calibrated microscopic measurements. Nevertheless, this approach does help with estimation of relative hyphal widths, even if they are subresolution objects, provided it is assumed that the intensity scales with the width of the hyphae (Fig. 7B). Including estimates of the hyphal width gives the volume of the mycelium at any point and, if time series are collected, how the volume changes with growth or recycling.

Conversion to a Graph Representation

The graph representation is based on translation of the pixel skeleton to a planar, weighted, undirected graph (Fig. 7C), with nodes located at hyphal tips, branches, and anastomoses, and edges representing hyphae or cords, with weights based on the Euclidean length (L) and radius (r) of each cord, combined either as the cylindrical volume ($V = \pi r^2 L$), to represent the material cost of the cord, or the predicted conductance ($G = r^2/L$), assuming cords are bundles of equally sized vessels rather than a single vessel with increasing radius (144, 173, 175, 182, 199–201). The network cannot be resolved within the resource, so it is represented as a single node connected to all the edges incident on the resource boundary (Fig. 7C). The graph conversion step also makes additional assumptions about the functional connectivity of the network, because every junction or crossing point is automatically defined as a fully connected node in 2-D planar systems irrespective of whether there is an actual anastomosis present, although 3-D imaging can help to separate fusions from overlaps (116). In addition, the inferred conductivity assumes all the septal pores are open and hyphae behave as simple pipes.

Summary statistics, such as the number of tips, junctions, and edges; the total hyphal length, area, and volume; or the distribution of branching angles and internodal lengths can be readily extracted from the pixel skeleton or graph representation of the fungal network (116, 144, 173, 175, 199–202). Measures can also be referenced to 2-D space to give tip densities and fractal dimensions (173, 175). Topological network measures, such as node degree, α-index or shortest path metrics, such as betweenness centrality (Fig. 7D), can also be readily calculated and show species-dependent developmental changes over time (144, 173, 199–203).

In more realistic microcosms with patchy resources, in competition with other species, or in the presence of
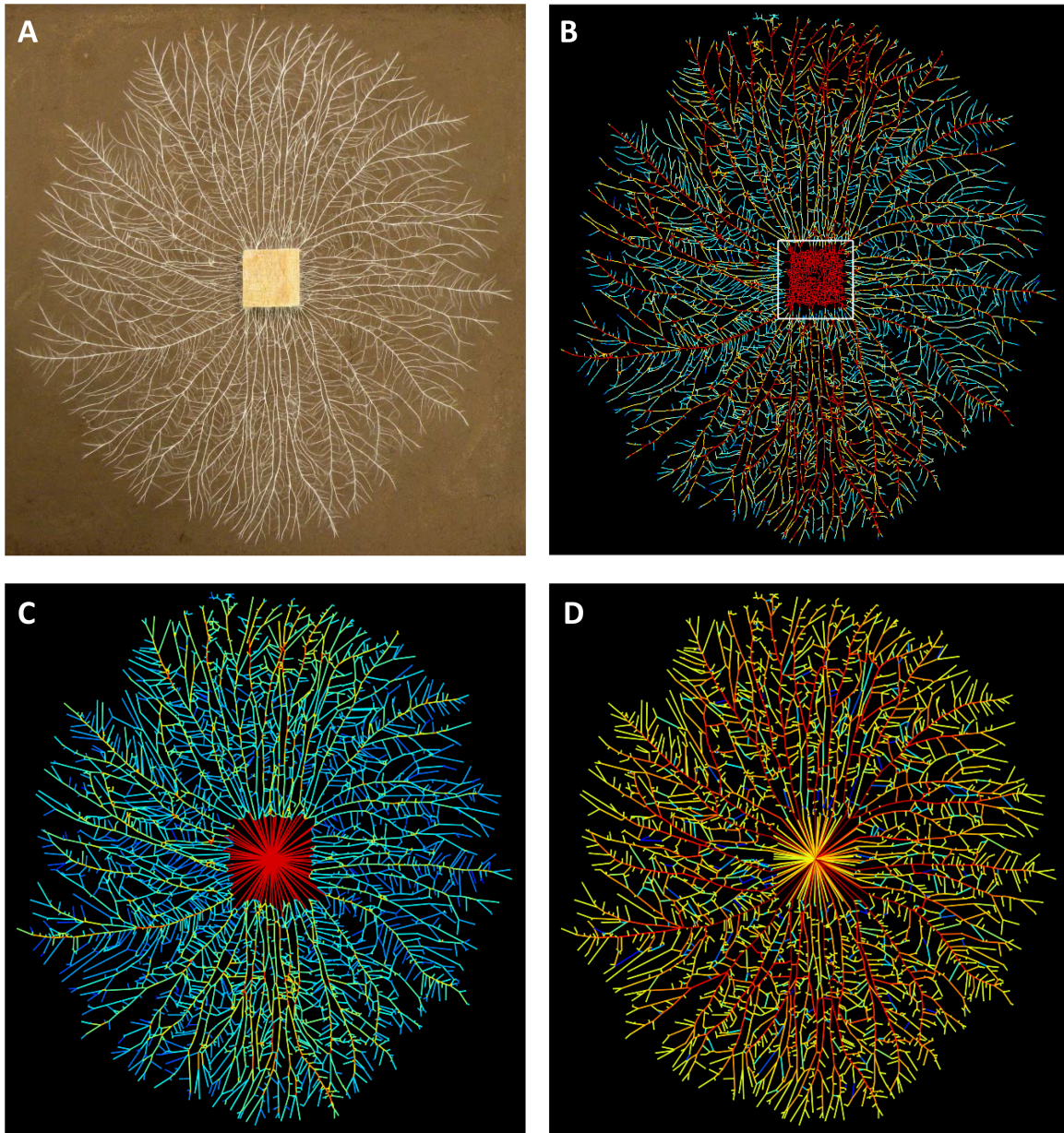
FIGURE 7 Macroscopic network analysis of *Phallus impudicus* growing on compressed soil. **(A)** Original image of the mycelial network after 21 days. **(B)** Network architecture automatically extracted using phase-congruency edge enhancement, watershed segmentation, and link pruning to give a single-pixel-wide skeleton pseudo-color coded by the cord width. **(C)** Conversion to a graph representation whereby each node (junction or tip) is connected by edges that are pseudo-color coded by the average width of the cord segment from 50 μm (blue) to 500 μm (red). The structure of the network within the wood resource cannot be defined so any cord incident on the boundary is connected to a central node with a link set to the maximum width. **(D)** Characterization of the cord betweenness centrality as a measure of how important each cord is to transport through the network from the resource to every other node, with the color code ranging from blue (low importance) to red (high importance).

fungivores, there is considerably more variation in spatial network architecture than is captured in a single summary network statistic. Such heterogeneity may be identified by algorithms that identify regions of the network with a higher local density of connections than other regions of the network than would be expected by chance, and are termed "communities" in network parlance. Communities are initially identified by progressively partitioning the network into smaller and smaller units by breaking links depending on the strength of their interaction, by tuning a resolution parameter. There is considerable flexibility in the choice of the interaction term that forms the basis of the analysis, which can be based on measures such as edge volume, conductance, or resilience ([204], [205]). The profile of key summary statistics, such as the number of communities, or the energy and entropy of the system, as the resolution parameter is changed, are used to define a set of mesoscopic response functions (MRFs) for each network. Networks are then clustered based on an estimate of the distance between the MRFs to give a dendrogram ([Fig. 8](#)). This provides a biologically sensible clustering of networks from different species, and also of developmental stages for a particular species, or exposure to different experi-

FIGURE 8 Network taxonomy. Taxonomies of 270 fungal (and slime mold) networks based on community structure using modularity optimization with path score (PS) values as the edge weights ([205](#)). The dendrogram was produced from the mesoscopic structure of each network as an indication of how similar different networks are to each other. The species abbreviations are coded as follows: Pp, *Physarum polycephalum*; Pv, *Phanerochaete velutina*; Ag, *Agrocybe gibberosa*; Pi, *Phallus impudicus*; Rb, *Resinicium bicolor*; and Sc, *Strophularia caerulea*. The levels of resources and amount of grazing are color coded from low (blue) to high (red). Substrate is coded as blue for agar, white for sand, and red for compressed, nonsterile soil. Interactions are coded as blue for no interaction, or red grown in competition with *Hypholoma fasciculare*. At the bottom of the figure, the logarithms of number of nodes N, number of edges M, and the edge density $\rho = 2M/N(N-1)$ are also shown. From reference [205](#) with permission.
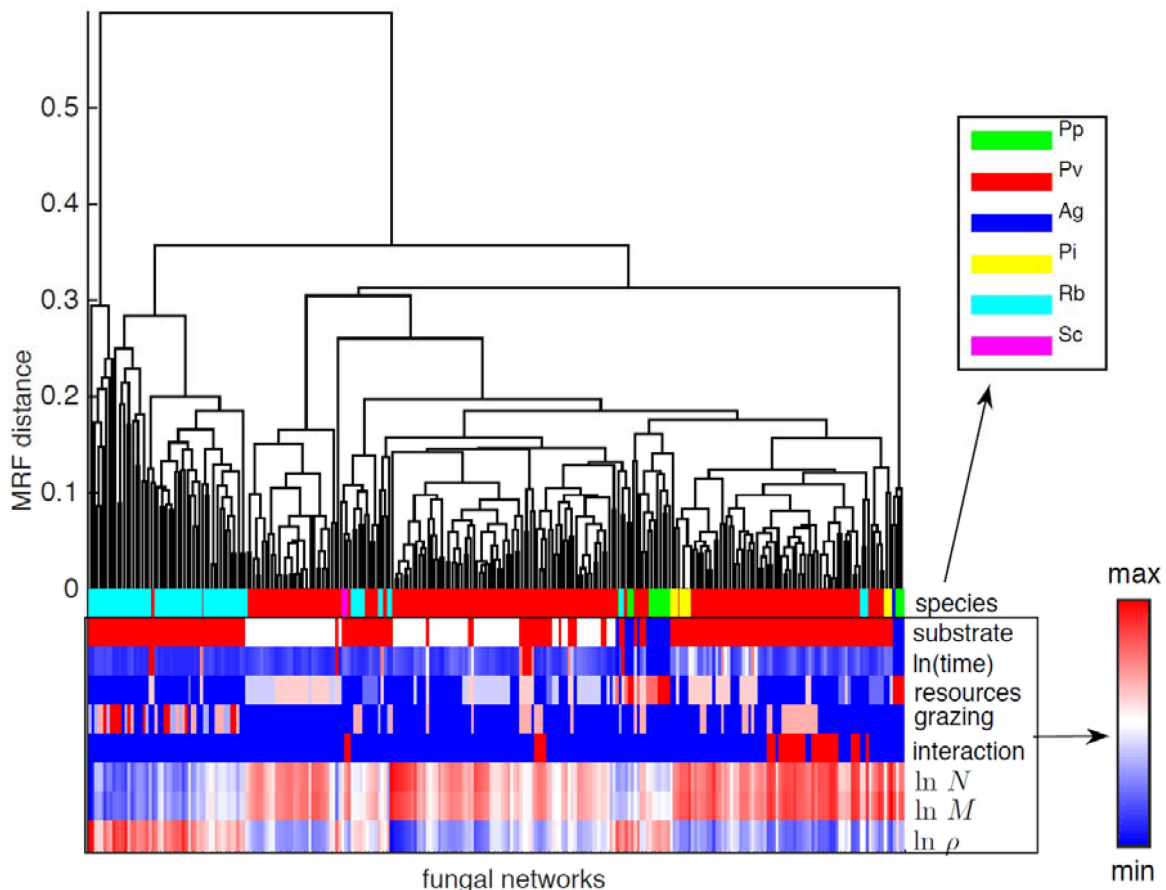
mental conditions ([204](#), [205](#)). These approaches allow objective groupings of networks across species, treatments, and laboratories. Nevertheless, these methods are in their infancy and the challenge now is to understand whether the groupings can be interpreted from a biological perspective to yield additional insight that cannot be captured from qualitative description of each network alone.

Integrating Structure and Flows Using Modeling

Constructing models that meaningfully represent processes ranging from the micron scale in individual hyphae to hyphal networks operating at an ecologically relevant scale is extremely challenging. At the microscopic scale, sophisticated biophysical models have been developed to explain the growth of individual hyphal tips, including vesicle delivery and viscoelastic wall deformation ([42](#), [206](#)–[211](#)), followed by wall aging through cross-linking of wall polymers ([4](#), [212](#), [213](#)). While, at a macroscopic scale, the growth of fungi in the environment can be modeled by using differential equations to represent changes in the density of fungal mycelia and spore production, along with changing resource density. Such an approach can be effective for modeling the spread of fungal crop pathogens ([214](#)), or modeling carbon cycling in the environment ([215](#)), but these kinds of model are essentially blind to the fact that fungal biomass grows as an interconnected network. Here, we consider an intermediate scale, namely the growth of individual mycelial networks.

Continuum Models at the Colony Level

One strategy for modeling the interaction between tips, hyphae, growth-limiting nutrients, and inhibitory waste products is to represent the mycelium as a continuum and use differential equations to model processes such as the uptake of nutrients by hyphae, the extension of tips to form hyphae, the formation of new tips through branching, and the loss of tips because of anastomosis. Such models have their roots in the work of Edelstein and coworkers ([216](#)), and they have been reasonably successful in explaining the gross morphology of colonies with dense mycelia, which can be observed growing on agar, plant surfaces, or building materials. For example, when *Aspergillus orzae* grows on agar, the morphology of the colony depends on the concentrations of nutrient and agar ([217](#), [218](#)). At low nutrient concentrations, colonies are uniform with a smooth, circular growth front provided that it is difficult for nutrients and waste products to diffuse through the agar.

If the agar concentration is decreased, the effective diffusion coefficient of waste products and nutrients is increased, and colonies condense into branched forms, with a tortuous, irregular growth front. This morphological instability can be explained by constructing a reaction-diffusion type model that takes into account the build-up of waste inhibitors and the provision of growth-limiting nutrients. Essentially, if the nutrients needed for growth can only be obtained by growing into new territory, a low-density colony will gradually fill the dish, maintaining circular symmetry. If nutrients can diffuse into already colonized regions, this will enable denser growth. However, in that case the buildup of inhibitory molecules can prevent some regions from growing out of the dense core, and any point on the growth front that happens to be further away from the inhibitory core will be more likely to grow, producing positive feedback and an unstable, irregular growth front.

Including Biomass Recycling in Continuum Models

Another feature of fungal physiology that can be incorporated into continuum models is the distinction between mobile and immobile fungal biomass. Metabolically active hyphal tips mature into relatively inert hyphae, or fully vacuolated vessels that are not metabolically active. Uptake of nutrients is generally believed to be greatly reduced behind the hyphal tips, and, in some species, hyphae develop into cords or metabolically inert transport vessels that are highly insulated from the environment ([17](#), [35](#), [219](#)). Although some biomass is static, the cytoplasmic contents of the fungal colony is free to move by pressure-driven mass flows, diffusion, or various mechanisms of active transport. Furthermore, some internal resources may be remobilized, as parts of the fungal colony are broken down and recycled to fuel further growth (see "Biomass recycling" above). Energetic arguments suggest that the process of recycling is of much greater benefit to organisms that live on recalcitrant or nutrient-poor substrates ([31](#)), and modeling suggests that the rate of recycling may also have a significant impact on colony morphology ([142](#)). There are three extreme morphologies: (i) "fairy rings," with an annulus of high-density growth surrounding a region with low or zero density; (ii) colonies of relatively constant density; or (iii) rings that alternate between higher and lower densities ([220](#); see "Colony dynamics and behavior" above). The distribution of densities of fungal growth depends on both the nutrient environment and the species in question, and models indicate the importance of nutrient transport and biomass recycling

in determining such morphologies ([24](#), [26](#), [142](#)). The fact that fungal growth is space filling is critically important, because the capacity to take up nutrients, water, or pollutants from the environment is proportional to the surface area. There is no reason to suppose that the total surface area of a fungal colony is a simple function of its diameter, which suggests that fungal growth and its environmental consequences may not be well represented by assuming some density of growth. One approach is to represent the space-filling capacity of fungi in terms of fractal dimension ([188](#), [221](#)–[224](#)) as the dimension of a space will influence the dynamics of any exchange process ([225](#)) (see "Fractal measures and hyphal coverage" above).

Spatially Explicit Network Models

A promising but computationally intensive approach is to adopt a spatially explicit representation of all the hyphae in a network ([26](#), [29](#), [226](#)). Each hyphal tip can be associated with a location and a direction, and the movement of those tips can be modeled so that tip velocity and changes in tip direction recapitulate empirical observations. These agent-based models can either be constrained to a lattice, or, at the expense of additional computational cost, the orientation of hyphal tips can be lattice free ([28](#), [30](#)). In all such "tip-and-trail" models, hyphae are present wherever the moving tips have passed, and those locations can be given traits such as internal and external concentration of growth-limiting resource. This approach enables the modeling of hyphal fusion, which is assumed to occur whenever a tip grows into a location that is already occupied by hyphae or tips.

Branching angle can also be modeled to recapitulate empirical observation, but there are fundamental difficulties in modeling branching frequency. One approach is to simply impose the distribution between branch points that has been observed experimentally ([226](#)). This may be appropriate when branching rate is constant and all branching events are apical or subapical because in that case it is relatively easy to measure branching frequency and the location of branching events is relatively well determined. Such a model can be used to determine the relationship between branching rate, branching angle, and the expected distribution of fungal density for colonies of various sizes ([226](#)), but in cases where the environment is heterogeneous and branching rate is not constant, it is not clear which branching rate should be imposed. An alternate approach is to suppose that tip growth and branching rate are a function of the internal concentration of some growth-limiting resource ([29](#),

[227](#)). Such models effectively reveal the importance of nutrient transport, but the internal concentration of nutrients will depend on the scale and mechanisms of nutrient uptake and translocation about which we still have little quantitative information ([16](#), [56](#), [147](#), [228](#)). Thus, it is not clear whether these models represent the mechanisms of nutrient transport with sufficient accuracy, nor is it clear whether they capture the actual relationship between branching rates and local conditions. Crucially, the connected nature of mycelial networks means that local behavior can be affected by conditions in remote parts of the colony, especially by the translocation of nutrients ([32](#), [219](#), [229](#), [230](#)).

Furthermore, because the flow of cytoplasmic contents is relatively unimpeded, turgor pressure will tend to equalize rapidly across the colony. Hence, turgor pressure and the rate of water uptake necessarily reflect the osmotic potential of the entire colony and its environment, not just the local conditions ([49](#), [231](#)). This implies that the behavior of the colony is dependent on the interaction between the genotype and a complex spatial convolution of environmental conditions ([26](#), [142](#), [232](#), [233](#)). It should also be noted that not all cords are equally important when a dynamic process occurs on a network. In a heterogeneous environment some cords will carry more resources than other, nearby edges ([28](#)), and empirical observations confirm that the distribution of velocities of fluid flow within a fungal network are highly heterogeneous, with some cords carrying much larger mass flows than others ([32](#), [33](#), [67](#)). This heterogeneity is presumably related to the fact that some hyphae branch and form hyphal aggregates or cords, while other hyphae are degraded and recycled. There is some evidence that cords which carry greater currents are more likely to thicken ([33](#)), but there is a substantial body of open questions concerning the developmental logic of fungal networks.

Comparison with Other Types of Transportation Networks

Given the importance of nutrient transport, it is worth considering how fungal networks compare with other transportation networks ([32](#), [144](#), [219](#)). In particular, modeling may be able to shed some light on the trade-offs involved in forming cross-links, because it is notable that some fungal networks contain numerous loops, while other fungi essentially grow as branching trees ([16](#), [199](#), [201](#)). There is a considerable literature on the optimal design of distribution networks, and fractal branching trees are known to be optimal for the case where a single source is connected to multiple sinks

(234–236). Furthermore, when a metabolism-limiting resource is distributed through a fractal branching tree, we should expect to see scaling effects such that larger organisms have a lower metabolic rate. As theory predicts, there is evidence in the animal kingdom that metabolic rate is proportional to $M^{3/4}$, where M represents the mass of the animal (234, 235). However, while mammals use a cardiovascular system to distribute oxygen, glucose, and other metabolism-limiting substances throughout the body from a single heart, fungal colonies generally cannot be represented as a single-source system. Nutrients may be gathered from across the colony, and such organisms may thrive by foraging phosphate from one location and nitrogen from another, and distributing both resources throughout the mycelium (147, 219). Hence, in the case of fungi, the distance that determines the scale of the transport challenge is not the radius or the mass of the colony, but the typical distance between the site of nutrient uptake and the place where those nutrients are consumed.

Whatever the spatial distribution of sources and sinks, any efficient flow pattern must be such that, at every point, the flow moves materials away from the source and toward the sink. In other words, although there may be loops in the network, optimally efficient flows always transport materials in a directed manner. This feature of efficient material flows is common to many definitions of "efficient," and it is inevitable when the flows are driven by differences in potential. That is because, at every point in any given network, material moves from regions of high potential to low potential. Hence, material can never backtrack, because that would require movement against the potential gradient. However, although it is most efficient for particles to move in a directed manner, there are circumstances in which the most efficient network is one that contains loops. In particular, if a network has to function in the face of random damage, or a network needs to connect a fluctuating distribution of sources and sinks, the most efficient choice of the network may be one that contains loops (237). Further modeling may help to elucidate the trade-offs that arise between the conflicting demands of efficient directed transport and efficient mixing. In many cases, the primary interest is in the functional consequences of fungal growth, such as the production rate of desirable compounds, the rate of nutrient or pollutant uptake, rates of soil acidification, wood degradation, and so on (227). Some of these macroscopic rates of interest have been connected to microscopic fungal parameters, such as branching rate or fungal density, but more effective predictive models may require a deeper

understanding of how fungal development shapes and responds to the environment in which growth occurs. The increasingly quantitative nature of experimental data concerning tip growth, branching, nutrient transport, and cytoplasmic flow should provide valuable material for future modeling efforts (116), and advances in imaging technology will surely enable a more detailed analysis of the architecture and functional significance of developing fungal networks.

Network Robustness and Resilience

In natural environments mycelial networks are subject to physical damage and attack by fungivores. The intrinsic robustness of the network at a particular time point is determined by the network architecture, including thickness and toughness of hyphae and mycelial cords, palatability to grazers, and extent of interconnectedness. In particular, networks with loops formed by anastomosis are more robust, because they already maintain alternative routes for nutrient translocation to circumvent damaged regions. Fungi can also respond to damage or attack by network remodeling leading to greater resilience. Experiments can be conducted with real networks in the presence of fungivores, or by using an *in silico* approach based on network analysis in other domains, whereby a property of the network, such as the largest connected component or the predicted transport efficiency, is calculated as cords are removed according to some rule. Thus, long thin cords might be removed first to simulate grazing by collembola with small mouth parts, or a local region of the network might be deleted as a chunk to simulate grazing by wood lice.

Experiments in Soil Microcosms

The effects of invertebrates grazing on mycelia of cord-forming wood decay basidiomycetes have been studied extensively in microcosms (24 × 24 cm or 50 × 50 cm) of compressed nonsterile woodland soil (238–240). Intense grazing can completely destroy mycelia and prevent them from growing out of organic resources, but less intense grazing can dramatically alter mycelial morphology and physiology, in different ways depending on the grazing species, the fungus, and the grazing intensity. Mycelia are grazed in different regions and to different extents depending on fungal species: collembola grazing on the relatively unpalatable *H. fasciculare* tends to be at hyphal tips; in contrast, *R. bicolor* extending from beech wood is indiscriminately grazed, and, with *P. velutina*, fine hyphae within the colony and hyphal tips are grazed (241). While microfauna and mesofauna often graze on fine hyphae, macrofauna such as woodlice (*Oniscus*

asellus) graze in large swathes including severing thick cords (242).

Susceptibility to grazing also depends on the age and stage of development of the mycelium and the resources to which it has access. Mycelia comprising individual hyphae or thin cords, at early stages of development or supported by a dearth of resources, are more prone to grazing than mycelia that have formed highly sclerotized cords interconnecting between woody resources (170, 239). Mycelial systems occupying large (50 × 50 cm) trays of soil had similar hyphal coverage after several months irrespective of whether or not they had been grazed by collembola (170), apparently because collembola grazed on the fine hyphae that would have died anyway as the system became more open. Greater mycelial interconnectedness, i.e., more cross-links forming tangential connections, also limits the effects of grazing and other damage (Fig. 5 and 9) (169, 243). Connectedness is greater in some species than others, e.g., greater in *Phallus impudicus* than *P. velutina* (see above), in mycelia developing from larger resources and in more mature systems (144, 169, 243, 244).

Effects of grazing depend not only on the intrinsic robustness but also on how mycelia respond to damage or grazing, i.e., resilience. Although extension rate often decreases as a result of invertebrate grazing (239), it sometimes increases, switching from slow, exploitative to fast, explorative growth (242). These changes sometimes occur at or close to the site of grazing, further away, and in all directions around a mycelial margin. The latter is invertebrate density dependent (239) and has been interpreted as compensatory growth, similar to that which occurs in plants during herbivory (238). During interactions between mycelia of *P. velutina* and *H. fasciculare* growing across soil, grazing by collembola curtailed growth of the former except in the region of the opponent, where rate of overgrowth rapidly increased (243). Remarkably, although collembola grazing of *P. velutina* tends to reduce interstitial hyphal biomass overall, some of these fine hyphae survive, and thicken, increasing the local level of cross-connectivity, and hence increasing robustness (169).

Network Risks: Control of Systemic Infection

Network organization may be useful for long-distance transport and coordinated colony behavior, but also poses a risk of rapid systemic infection. Indeed, approximately 30 to 80% of fungi are thought to harbor persistent systemic mycovirus infections that spread horizontally via hyphal anastomosis between compatible fungal hosts, or vertically through spore formation, with no extracellular mode of infection (245, 246).
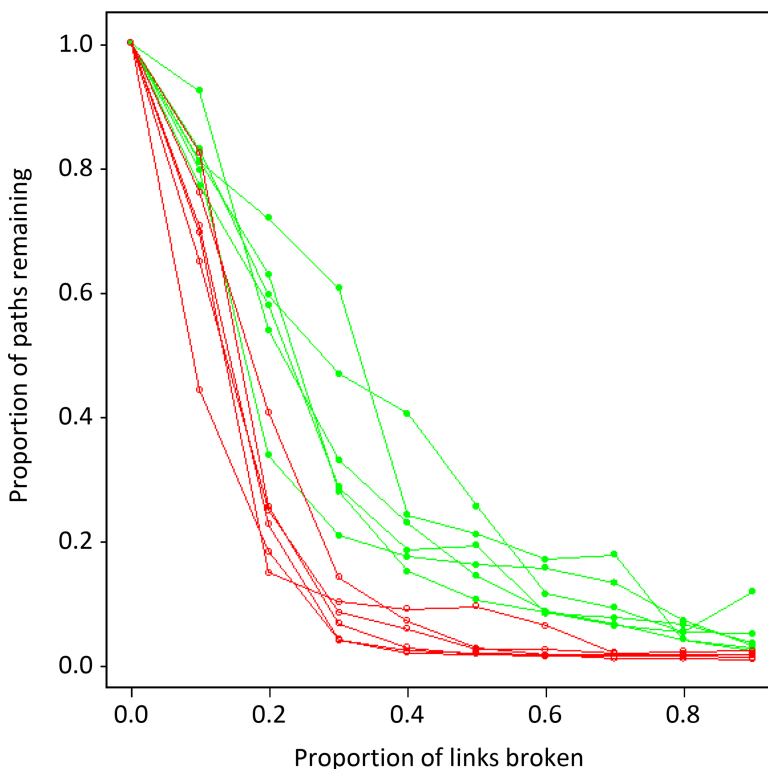
FIGURE 9 *In silico* evaluation of network robustness. Networks of *Phanerochaete velutina* (red) and *Phallus impudicus* (green) were attacked *in silico* by progressively removing links in the network at random, and calculating the number of paths in the network that still remain. In each case, five examples are shown. Note that the *P. velutina* network breaks down more rapidly than the *P. impudicus*. From D. A'Bear, L. Boddy, and M. D. Fricker, unpublished data.

FUTURE PROSPECTS

Extension of Network Analysis to 3-D

It is already possible to collect sets of tiled 3-D confocal images of fungi growing on agar with sufficient resolution to identify individual hyphae, and sufficient spatial and temporal scales to map colony development over a period of days, which gives a much richer source of information for modeling (116). Recent progress has also been made on 3-D imaging of fungi in wood or soil with sub-micron resolution using X-ray computed tomography (247–250). However, manual or automated segmentation and analysis routines are still challenging, as the invasive hyphae can be very narrow and it is currently difficult to achieve sufficient contrast to segment fungal hyphae from the woody tissue (247, 248, 250). Imaging mycelial networks in soil has used osmium vapor staining and use of X-ray translucent polystyrene substrate to create sufficient contrast (249). Nevertheless, at this point, it is not possible to extract a connected 3-D network from either substrate, but it is anticipated that further methodological improvements will overcome some of the current technological challenges.

Intercellular and intracellular hyphal networks formed during host-mycorrhizal interactions have been successfully imaged at cellular resolution using confocal micros-copy after labeling with various fluorophores (133, 251–253), using label-free imaging (254), by *in situ* hybridization (255), or following combined KOH maceration, resin embedding, physical sectioning, and confocal imaging of fluorescently labeled wheat germ agglutinin lectin (256, 257). Quantitative measurements of volumes and surface areas are possible, even from dense arbuscules (251). Techniques to visualize arbuscular mycorrhizal networks by sandwiching between Millipore filters give impressive images of the mycelial network and have allowed quantitation of hyphal lengths and number of anastomoses (258, 259), and could easily be subject to network analysis. Likewise, cord-forming ectomycorrhizal networks can be imaged and analyzed by using the same approaches developed for saprotrophic systems (Fig. 10), although it is more complex to segment the fungal mycelium from the root because they span different scales and the color discrimination from each other and the soil is difficult.

In a similar manner, pathogens invading their host can be labeled by using nonspecific stains or fluorochromes or by following expression of fluorescent proteins (260–262). Lesion development can be followed by automated segmentation and analysis by using the HyphArea program (191), which has the potential to provide a com-

FIGURE 10 Network analysis of the ectomycorrhizal fungus *Paxillus* on pine. **(A)** *Pinus* seedling infected with *Paxillus*. The dotted white circle marks the loading site for radioactive ^{14}C-AIB. The dotted red lines indicate the routes for preferential transport of isotope to the roots from C. **(B)** Automated extraction of both the plant root and extra-radical mycorrhizal network using phase-congruency enhancement, watershed segmentation, and cord width measurement. **(C)** Scintillation image of nutrient movement along selected pathways from the fungus to the plant root. From R. Tajuddin, D. Johnson, and M.D. Fricker, unpublished data.
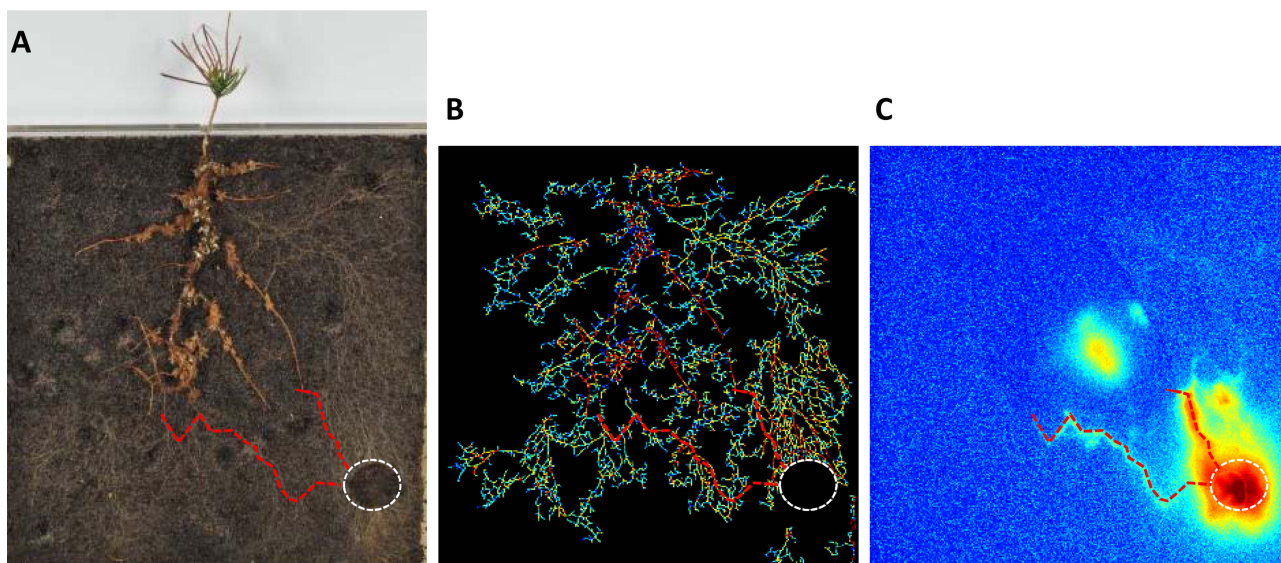
plete, quantitative representation of the invasive hyphal network. The length scale that most pathogen infections operate over is quite limited (millimeters to centimeters), which suggests that growth and internal nutrient movement can be accomplished easily by diffusion and cytoplasmic streaming rather than by mass flow.

Network Analysis and Fitness Traits

The network formed by different species is recognizable at a macroscopic level, and tools to quantify network architecture and dynamics are emerging. At this point, we do not know which metrics may best describe network organization and how these relate to fitness (263), but it is not unreasonable to propose that each species operates a slightly different set of local rules to balance growth, transport efficiency, recycling, resilience, and reproduction that collectively maximize the long-term global success of the organism (31, 264). Thus, network analysis may help to provide quantitative measures of traits that fulfill the criteria of ecological versatility, wide scope throughout the fungal kingdom, and measurability set out by Aguilar-Trigeros et al. (39).

REFERENCES

1. **Buller AHR.** 1924. *Researches on Fungi*, vol 3. Longmans Green, London, United Kingdom.

2. **Buller AHR.** 1931. *Researches on Fungi*, vol 4. Longmans Green, London, United Kingdom.

3. **Buller AHR.** 1933. *Researches on Fungi*, vol 5. Longmans Green, London, United Kingdom.

4. **Riquelme M.** 2013. Tip Growth in Filamentous Fungi: A Road Trip to the Apex. *Annu Rev Microbiol* **67:**587–609.

5. **Mouriño-Pérez RR, Riquelme M.** 2013. Recent advances in septum biogenesis in *Neurospora crassa*. *Adv Genet* **83:**99–134.

6. **Jedd G.** 2011. Fungal evo-devo: organelles and multicellular complexity. *Trends Cell Biol* **21:**12–19.

7. **Brand A, Gow NAR.** 2009. Mechanisms of hypha orientation of fungi. *Curr Opin Microbiol* **12:**350–357.

8. **Harris SD.** 2008. Branching of fungal hyphae: regulation, mechanisms and comparison with other branching systems. *Mycologia* **100:**823–832.

9. **Read ND, Fleißner A, Roca GM, Glass NL.** 2010. Hyphal fusion, p 260–273. *In* Borkovich KA, Ebbole D (ed), *Cellular and Molecular Biology of Filamentous Fungi*. American Society for Microbiology, Washington, DC.

10. **Glass NL, Rasmussen C, Roca MG, Read ND.** 2004. Hyphal homing, fusion and mycelial interconnectedness. *Trends Microbiol* **12:**135–141.

11. **Fleißner A, Herzog S.** 2016. Signal exchange and integration during self-fusion in filamentous fungi. *Semin Cell Dev Biol* **57:**76–83.

12. **Weichert M, Fleißner A.** 2015. Anastomosis and Heterokaryon Formation, p 3–21. *In* van den Berg MA, Maruthachalam K (ed), *Genetic Transformation Systems in Fungi*, vol 2. Springer International Publishing, Cham, Switzerland. doi:10.1007/978-3-319-10503-1_1.

13. **Herzog S, Schumann MR, Fleißner A.** 2015. Cell fusion in *Neurospora crassa*. *Curr Opin Microbiol* **28:**53–59.

14. **Olsson S.** 2001. Colonial growth of fungi, p 125–141. *In* Howard RJ, Gow NAR (ed), *Biology of the Fungal Cell*, vol 8. Springer, Berlin, Germany.

15. **Jennings DH.** 1987. Translocation of solutes in fungi. *Biol Rev Camb Philos Soc* **62:**215–243.

16. **Heaton L, Obara B, Grau V, Jones N, Nakagaki T, Boddy L, Fricker MD.** 2012. Analysis of fungal networks. *Fungal Biol Rev* **26:**12–29.

17. **Cairney JWG.** 1992. Translocation of solutes in ectomycorrhizal and saprotrophic rhizomorphs. *Mycol Res* **96:**135–141.

18. **Rayner ADM, Watkins ZR, Beeching JR.** 1999. Self-integration: an emerging concept from the fungal mycelium, p 1–24. *In* Gow NAR, Robson GD, Gadd GM (ed), *The Fungal Colony*. Cambridge University Press, Cambridge, United Kingdom.

19. **Rayner ADM, Griffith GS, Ainsworth AM.** 1994. Mycelial interconnectedness, p 21–40. *In* Gow NAR, Gadd GM (ed), *The Growing Fungus*. Chapman and Hall, London, United Kingdom.

20. **Rayner ADM.** 1991. The challenge of the individualistic mycelium. *Mycologia* **83:**48–71.

21. **Boswell GP, Jacobs H, Davidson FA, Gadd GM, Ritz K.** 2002. Functional consequences of nutrient translocation in mycelial fungi. *J Theor Biol* **217:**459–477.

22. **Boswell GP, Jacobs H, Davidson FA, Gadd GM, Ritz K.** 2003. Growth and function of fungal mycelia in heterogeneous environments. *Bull Math Biol* **65:**447–477.

23. **Boswell GP, Jacobs H, Davidson FA, Gadd GM, Ritz K.** 2003. A positive numerical scheme for a mixed-type partial differential equation model for fungal growth. *Appl Math Comput* **138:**321–340.

24. **Boswell GP, Jacobs H, Davidson F, Gadd GM, Ritz K, Davidson FA.** 2003. A mathematical approach to studying fungal mycelia. *Mycologist* **17:**165–171.

25. **Jacobs H, Boswell GP, Scrimgeour CM, Davidson FA, Gadd GM, Ritz K.** 2004. Translocation of carbon by *Rhizoctonia solani* in nutritionally-heterogeneous microcosms. *Mycol Res* **108:**453–462.

26. **Boswell GP, Jacobs H, Ritz K, Gadd GM, Davidson FA.** 2007. The development of fungal networks in complex environments. *Bull Math Biol* **69:**605–634.

27. **Davidson FA, Boswell GP, Fischer MW, Heaton L, Hofstadler D, Roper M.** 2011. Mathematical modelling of fungal growth and function. *IMA Fungus* **2:**33–37.

28. **Hopkins S, Boswell GP.** 2012. Mycelial response to spatiotemporal nutrient heterogeneity: a velocity-jump mathematical model. *Fungal Ecol* **5:**124–136.

29. **Boswell GP, Hopkins S.** 2009. Linking hyphal growth to colony dynamics: spatially explicit models of mycelia. *Fungal Ecol* **4:**143–154.

30. **Carver I, Boswell GP.** 2008. A lattice-free model of translocation-induced outgrowth in fungal mycelia. *IAENG Int J App Math* **38:**173–179.

31. **Heaton LLM, Jones NS, Fricker MD, Kerkhoff AJ, Kalisz S.** 2015. Energetic constraints on fungal growth. *Am Nat* **187:**E27–E40. 10.1086/684392:E000-E000.

32. **Heaton LL, López E, Maini PK, Fricker MD, Jones NS.** 2012. Advection, diffusion, and delivery over a network. *Phys Rev E Stat Nonlin Soft Matter Phys* **86:**021905.

33. **Heaton LLM, López E, Maini PK, Fricker MD, Jones NS.** 2010. Growth-induced mass flows in fungal networks. *Proc Biol Sci* **277:**3265–3274.

34. **Boddy L.** 1993. Saprotrophic cord-forming fungi: warfare strategies and other ecological aspects. *Mycol Res* **97:**641–655.

35. **Boddy L.** 1999. Saprotrophic cord-forming fungi: meeting the challenge of heterogeneous environments. *Mycologia* **91:**13–32.

36. **Fricker MD, Bebber DP, Boddy L.** 2008. Mycelial networks: structure and dynamics, p 3–18. *In* Boddy L, Franklin JC, van West P (ed), *Ecology of Saprotrophic Basidiomycetes*, vol 28. Academic Press, Amsterdam, The Netherlands.

37. **Simard SW, Beiler KJ, Bingham MA, Deslippe JR, Philip LJ, Teste FP.** Mycorrhizal networks: mechanisms, ecology and modelling. *Fungal Biol Rev* **26:**39–60.

38. **Horton TR.** 2015. *Mycorrhizal networks*, vol 224. Springer, Dordrecht, The Netherlands.

39. **Aguilar-Trigueros CA, Hempel S, Powell JR, Anderson IC, Antonovics J, Bergmann J, Cavagnaro TR, Chen B, Hart MM, Klironomos J, Petermann JS, Verbruggen E, Veresoglou SD, Rillig MC.** 2015. Branching out: towards a trait-based understanding of fungal ecology. *Fungal Biol Rev* **29:**34–41.

40. **Steinberg G.** 2014. Endocytosis and early endosome motility in filamentous fungi. *Curr Opin Microbiol* **20:**10–18.

41. **Steinberg G.** 2007. Hyphal growth: a tale of motors, lipids, and the Spitzenkörper. *Eukaryot Cell* **6:**351–360.

42. **Balmant W, Sugai-Guérios MH, Coradin JH, Krieger N, Furigo Junior A, Mitchell DA.** 2015. A model for growth of a single fungal hypha based on well-mixed tanks in series: simulation of nutrient and vesicle transport in aerial reproductive hyphae. *PLoS One* **10:**e0120307.

43. **Shoji JY, Kikuma T, Kitamoto K.** 2014. Vesicle trafficking, organelle functions, and unconventional secretion in fungal physiology and pathogenicity. *Curr Opin Microbiol* **20:**1–9.

44. **Steinberg G PM, Riquelme M, Wösten HA, Harris SD.** 2017. Cell biology of hyphal growth. *Microbiol Spectrum* **5**(2):FUNK-0034-2016. doi:10.1128/microbiolspec.FUNK-0034-2016.

45. **Davis DJ, Burlak C, Money NP.** 2000. Osmotic pressure of fungal compatible osmolytes. *Mycol Res* **104:**800–804.

46. **Brownlee C, Jennings DH.** 1981. The content of soluble carbohydrates and their translocation in mycelium of *Serpula lacrimans*. *Trans Br Mycol Soc* **77:**615–619.

47. **Money NP.** 2008. Insights on the mechanics of hyphal growth. *Fungal Biol Rev* **22:**71–76.

48. **Money NP.** 1997. Wishful thinking of turgor revisited: the mechanics of fungal growth. *Fungal Genet Biol* **21:**173–187.

49. **Lew RR.** 2011. How does a hypha grow? The biophysics of pressurized growth in fungi. *Nat Rev Microbiol* **9:**509–518.

50. **Emerson S.** 1964. Slime: a plasmodioid variant of *Neurospora crassa*. *Genetica* **34:**162–182.

51. **Olsson S, Jennings DH.** 1991. A glass-fiber filter technique for studying nutrient-uptake by fungi: the technique used on colonies grown on nutrient gradients of carbon and phosphorus. *Exp Mycol* **15:**292–301.

52. **Olsson S, Jennings DH.** 1991. Evidence for diffusion being the mechanism of translocation in the hyphae of three molds. *Exp Mycol* **15:**302–309.

53. **Darrah PR, Tlalka M, Ashford A, Watkinson SC, Fricker MD.** 2006. The vacuole system is a significant intracellular pathway for longitudinal solute transport in basidiomycete fungi. *Eukaryot Cell* **5:**1111–1125.

54. **Ashford AE, Allaway WG.** 2002. The role of the motile tubular vacuole system in mycorrhizal fungi. *Plant Soil* **244:**177–187.

55. **Ashford AE.** 1998. Dynamic pleiomorphic vacuole systems: are they endosomes and transport compartments in fungal hyphae? *Adv Bot Res* **28:**119–159.

56. **Olsson S.** 1995. Mycelial density profiles of fungi on heterogeneous media and their interpretation in terms of nutrient reallocation patterns. *Mycol Res* **99:**143–153.

57. **Schutte KH.** 1956. Translocation in the fungi. *New Phytol* **55:**164–182.

58. **Woolston BM, Schlagnhaufer C, Wilkinson J, Larsen J, Shi Z, Mayer KM, Walters DS, Curtis WR, Romaine CP.** 2011. Long-distance translocation of protein during morphogenesis of the fruiting body in the filamentous fungus, *Agaricus bisporus*. *PLoS One* **6:**e28412.

59. **Steinberg G, Schliwa M.** 1996. Characterization of the biophysical and motility properties of kinesin from the fungus Neurospora crassa. *J Biol Chem* **271:**7516–7521.

60. **Schott DH, Collins RN, Bretscher A.** 2002. Secretory vesicle transport velocity in living cells depends on the myosin-V lever arm length. *J Cell Biol* **156:**35–40.

61. **Steinberg G, Schliwa M.** 1993. Organelle movements in the wild-type and wall-less fz;sg;os-1 mutants of *Neurospora crassa* are mediated by cytoplasmic microtubules. *J Cell Sci* **106:**555–564.

62. **Goldstein RE, van de Meent J-W.** 2015. A physical perspective on cytoplasmic streaming. *Interface Focus* **5:**20150030.

63. **Thrower L, Thrower S.** 1968. Movement of nutrients in fungi. I. The mycelium. *Aust J Bot* **16:**71–80.

64. **Ramos-García SL, Roberson RW, Freitag M, Bartnicki-García S, Mouriño-Pérez RR.** 2009. Cytoplasmic bulk flow propels nuclei in mature hyphae of *Neurospora crassa*. *Eukaryot Cell* **8:**1880–1890.

65. **Roper M, Lee C, Hickey PC, Gladfelter AS.** 2015. Life as a moving fluid: fate of cytoplasmic macromolecules in dynamic fungal syncytia. *Curr Opin Microbiol* **26:**116–122.

66. **Lew RR.** 2005. Mass flow and pressure-driven hyphal extension in *Neurospora crassa*. *Microbiology* **151:**2685–2692.

67. **Roper M, Simonin A, Hickey PC, Leeder A, Glass NL.** 2013. Nuclear dynamics in a fungal chimera. *Proc Natl Acad Sci USA* **110:**12875–12880.

68. **Abadeh A, Lew RR.** 2013. Mass flow and velocity profiles in *Neurospora* hyphae: partial plug flow dominates intra-hyphal transport. *Microbiology* **159:**2386–2394.

69. **Pieuchot L, Lai J, Loh RA, Leong FY, Chiam K-H, Stajich J, Jedd G.** 2015. Cellular subcompartments through cytoplasmic streaming. *Dev Cell* **34:**410–420.

70. **Thompson W, Eamus D, Jennings DH.** 1985. Water flux through mycelium of *Serpula lacrimans*. *Trans Br Mycol Soc* **84:**601–608.

71. **Coggins CR, Jennings DH, Clarke RW.** 1980. Tear or drop formation by mycelium of *Serpula lacrimans*. *Trans Br Mycol Soc* **75:**63–67.

72. **Sun Y-P, Unestam T, Lucas SD, Johanson KJ, Kenne L, Finlay R.** 1999. Exudation-reabsorption in a mycorrhizal fungus, the dynamic interface for interaction with soil and soil microorganisms. *Mycorrhiza* **9:**137–144.

73. **Unestam T, Sun Y-P.** 1995. Extramatrical structures of hydrophobic and hydrophilic ectomycorrhizal fungi. *Mycorrhiza* **5:**301–311.

74. **Guhr A, Borken W, Spohn M, Matzner E.** 2015. Redistribution of soil water by a saprotrophic fungus enhances carbon mineralization. *Proc Natl Acad Sci USA* **112:**14647–14651.

75. **Cowan MC, Lewis BG, Thain JF.** 1972. Uptake of potassium by the developing sporangiophore of *Phycomyces blakesleeanus*. *Trans Br Mycol Soc* **58:**113–126.

76. **Allen MF.** 2007. Mycorrhizal fungi: highways for water and nutrients in arid soils. *Vadose Zone J* **6:**291–297.

77. **Dressaire E, Yamada L, Song B, Roper M.** 2016. Mushrooms use convectively created airflows to disperse their spores. *Proc Natl Acad Sci USA* **113:**2833–2838.

78. **Pringle A, Patek SN, Fischer M, Stolze J, Money NP.** 2005. The captured launch of a ballistospore. *Mycologia* **97:**866–871.

79. **Nobel PS.** 1991. *Physicochemical and Environmental Plant Physiology*. Academic Press, San Diego, CA.

80. **Soveral G, Veiga A, Loureiro-Dias MC, Tanghe A, Van Dijck P, Moura TF.** 2006. Water channels are important for osmotic adjustments of yeast cells at low temperature. *Microbiology* **152:**1515–1521.

81. **Dupont S, Lemetais G, Ferreira T, Cayot P, Gervais P, Beney L.** 2012. Ergosterol biosynthesis: a fungal pathway for life on land? *Evolution* **66:**2961–2968.

82. **Parks LW, Casey WM.** 1995. Physiological implications of sterol biosynthesis in yeast. *Annu Rev Microbiol* **49:**95–116.

83. **Dietz S, von Bülow J, Beitz E, Nehls U.** 2011. The aquaporin gene family of the ectomycorrhizal fungus *Laccaria bicolor*: lessons for symbiotic functions. *New Phytol* **190:**927–940.

84. **Pettersson N, Filipsson C, Becit E, Brive L, Hohmann S.** 2005. Aquaporins in yeasts and filamentous fungi. *Biol Cell* **97:**487–500.

85. **Nehls U, Dietz S.** 2014. Fungal aquaporins: cellular functions and ecophysiological perspectives. *Appl Microbiol Biotechnol* **98:**8835–8851.

86. **Verma RK, Prabh ND, Sankararamakrishnan R.** 2014. New subfamilies of major intrinsic proteins in fungi suggest novel transport properties in fungal channels: implications for the host-fungal interactions. *BMC Evol Biol* **14:**173.

87. **Fricke W.** 2015. The significance of water co-transport for sustaining transpirational water flow in plants: a quantitative approach. *J Exp Bot* **66:**731–739.

88. **Wegner LH.** 2014. Root pressure and beyond: energetically uphill water transport into xylem vessels? *J Exp Bot* **65:**381–393.

89. **Bayry J, Aimanianda V, Guijarro JI, Sunde M, Latgé J-P.** 2012. Hydrophobins—unique fungal proteins. *PLoS Pathog* **8:**e1002700.

90. **Wessels J, De Vries O, Asgeirsdottir SA, Schuren F.** 1991. Hydrophobin genes involved in formation of aerial hyphae and fruit bodies in *Schizophyllum. Plant Cell* **3:**793–799.

91. **Wosten H, De Vries O, Wessels J.** 1993. Interfacial self-assembly of a fungal hydrophobin into a hydrophobic rodlet layer. *Plant Cell* **5:**1567–1574.

92. **Bell AA, Wheeler MH.** 1986. Biosynthesis and functions of fungal melanins. *Annu Rev Phytopathol* **24:**411–451.

93. **Money NP.** 1990. Measurement of pore-size in the hyphal cell-wall of *Achlya bisexualis. Exp Mycol* **14:**234–242.

94. **Simard S, Asay A, Beiler K, Bingham M, Deslippe J, He X, Philip L, Song Y, Teste F.** 2015. Resource transfer between plants through ectomycorrhizal fungal networks, p 133–176. *In:* Horton TR (ed), *Mycorrhizal Networks*. Springer, Dordrecht, The Netherlands.

95. **Casadevall A, Nosanchuk JD, Williamson P, Rodrigues ML.** 2009. Vesicular transport across the fungal cell wall. *Trends Microbiol* **17:**158–162.

96. **Lutzoni F, Kauff F, Cox CJ, McLaughlin D, Celio G, Dentinger B, Padamsee M, Hibbett D, James TY, Baloch E, Grube M, Reeb V, Hofstetter V, Schoch C, Arnold AE, Miadlikowska J, Spatafora J, Johnson D, Hambleton S, Crockett M, Shoemaker R, Sung G-H, Lücking R, Lumbsch T, O'Donnell K, Binder M, Diederich P, Ertz D, Gueidan C, Hansen K, Harris RC, Hosaka K, Lim Y-W, Matheny B, Nishida H, Pfister D, Rogers J, Rossman A, Schmitt I, Sipman H, Stone J, Sugiyama J, Yahr R, Vilgalys R.** 2004. Assembling the fungal tree of life: progress, classification, and evolution of subcellular traits. *Am J Bot* **91:**1446–1480.

97. **Jedd G, Pieuchot L.** 2012. Multiple modes for gatekeeping at fungal cell-to-cell channels. *Mol Microbiol* **86:**1291–1294.

98. **Ng SK, Liu F, Lai J, Low W, Jedd G.** 2009. A tether for Woronin body inheritance is associated with evolutionary variation in organelle positioning. *PLoS Genet* **5:**e1000521.

99. **Bleichrodt RJ, van Veluw GJ, Recter B, Maruyama J, Kitamoto K, Wösten HAB.** 2012. Hyphal heterogeneity in *Aspergillus oryzae* is the result of dynamic closure of septa by Woronin bodies. *Mol Microbiol* **86:**1334–1344.

100. **Samalova M, Meyer AJ, Gurr SJ, Fricker MD.** 2014. Robust antioxidant defences in the rice blast fungus *Magnaporthe oryzae* confer toleranceto the host oxidative burst. *New Phytol* **201:**556–573. doi:10.1111/nph.12530.

101. **van Peer AF, Müller WH, Boekhout T, Lugones LG, Wösten HAB.** 2009. Cytoplasmic continuity revisited: closure of septa of the filamentous fungus *Schizophyllum commune* in response to environmental conditions. *PLoS One* **4:**e5977.

102. **Prosser JI, Trinci APJ.** 1979. Model for hyphal growth and branching. *J Gen Microbiol* **111:**153–164.

103. **Hayakawa Y, Ishikawa E, Shoji JY, Nakano H, Kitamoto K.** 2011. Septum-directed secretion in the filamentous fungus *Aspergillus oryzae. Mol Microbiol* **81:**40–55.

104. **Sherman TF.** 1981. On connecting large vessels to small: the meaning of Murray's law. *J Gen Physiol* **78:**431–453.

105. **Kamiya A, Bukhari R, Togawa T.** 1984. Adaptive regulation of wall shear stress optimizing vascular tree function. *Bull Math Biol* **46:**127–137.

106. **Lichius A, Goryachev AB, Fricker MD, Obara B, Castro-Longoria E, Read ND.** 2014. CDC-42 and RAC-1 regulate opposite chemotropisms in *Neurospora crassa. J Cell Sci* **127:**1953–1965.

107. **Read ND.** 2011. Exocytosis and growth do not occur only at hyphal tips. *Mol Microbiol* **81:**4–7.

108. **Voisey CR.** 2010. Intercalary growth in hyphae of filamentous fungi. *Fungal Biol Rev* **24:**123–131.

109. **Katz D, Goldstein D, Rosenberger RF.** 1972. Model for branch initiation in *Aspergillus nidulans* based on measurements of growth parameters. *J Bacteriol* **109:**1097–1100.

110. **Plomley NJB.** 1959. Formation of the colony in the fungus *Chaetomium. Aust J Biol Sci* **12:**53–64.

111. **Trinci APJ.** 1971. Influence of width of peripheral growth zone on radial growth rate of fungal colonies on solid media. *J Gen Microbiol* **67:**325–344.

112. **Morrison KB, Righelato RC.** 1974. The relationship between hyphal branching, specific growth rate and colony radial growth rate in *Penicillium chrysogenum. J Gen Microbiol* **81:**517–520.

113. **Koch AL.** 1975. The kinetics of mycelial growth. *J Gen Microbiol* **89:**209–216.

114. **Gow NAR, Gooday GW.** 1982. Growth kinetics and morphology of colonies of the filamentous form of *Candida albicans. J Gen Microbiol* **128:**2187–2194.

115. **Ritz K.** 1995. Growth responses of some soil fungi to spatially heterogeneous nutrients. *FEMS Microbiol Ecol* **16:**269–279.

116. **Du H, Lv P, Ayouz M, Besserer A, Perré P.** 2016. Morphological characterization and quantification of the mycelial growth of the brown-rot fungus *Postia placenta* for modeling purposes. *PLoS One* **11:**e0162469.

117. **Prosser JI.** 1993. Growth kinetics of mycelial colonies and aggregates of Ascomycetes. *Mycol Res* **97:**513–528.

118. **Akiyama K, Matsuzaki K, Hayashi H.** 2005. Plant sesquiterpenes induce hyphal branching in arbuscular mycorrhizal fungi. *Nature* **435:**824–827.

119. **Trinci APJ, Collinge A.** 1973. Influence of L-sorbose on the growth and morphology of *Neurospora crassa. J Gen Microbiol* **78:**179–192.

120. **Riquelme M, Bartnicki-Garcia S.** 2004. Key differences between lateral and apical branching in hyphae of *Neurospora crassa. Fungal Genet Biol* **41:**842–851.

121. **Watters MK, Virag A, Haynes J, Griffiths AJF.** 2000. Branch initiation in *Neurospora* is influenced by events at the previous branch. *Mycol Res* **104:**805–809.

122. **Watters MK, Griffiths AJF.** 2001. Tests of a cellular model for constant branch distribution in the filamentous fungus *Neurospora crassa. Appl Environ Microbiol* **67:**1788–1792.

123. **Fleissner A, Sarkar S, Jacobson DJ, Roca MG, Read ND, Glass NL.** 2005. The *so* locus is required for vegetative cell fusion and post-fertilization events in *Neurospora crassa. Eukaryot Cell* **4:**920–930.

124. **Simonin A, Palma-Guerrero J, Fricker M, Glass NL.** 2012. Physiological significance of network organization in fungi. *Eukaryot Cell* **11:**1345–1352.

125. **Olsson S, Gray S.** 1998. Patterns and dynamics of ^{32}P-phosphate and labelled 2-aminoisobutyric acid (^{14}C-AIB) translocation in intact basidiomycete mycelia. *FEMS Microbiol Ecol* **26:**109–120.

126. Agerer R. 2007. Diversity of ectomycorrhizae as seen from below and above ground: the exploration types. *Z Mykol* **73:**61.

127. Agerer R. 2006. Fungal relationships and structural identity of their ectomycorrhizae. *Mycol Prog* **5:**67–107.

128. Cairney JWG. 1991. Rhizomorphs: organs of exploration or exploitation? *Mycologist* **5:**5–10.

129. Butler GM. 1958. The development and behaviour of mycelial strands in *Merulius lacrymans* (Wulf.) Fr. II. Hyphal behaviour during strand formation. *Ann Bot (Lond)* **22:**219–236.

130. Brownlee C, Jennings DH. 1982. Pathway of translocation in *Serpula lacrimans. Trans Br Mycol Soc* **79:**401–407.

131. Tlalka M, Hensman D, Darrah PR, Watkinson SC, Fricker MD. 2003. Noncircadian oscillations in amino acid transport have complementary profiles in assimilatory and foraging hyphae of *Phanerochaete velutina. New Phytol* **158:**325–335.

132. Tlalka M, Watkinson SC, Darrah PR, Fricker MD. 2002. Continuous imaging of amino-acid translocation in intact mycelia of *Phanerochaete velutina* reveals rapid, pulsatile fluxes. *New Phytol* **153:**173–184.

133. Schweiger PF, Rouhier H, Soderstrom B. 2002. Visualisation of ectomycorrhizal rhizomorph structure using laser scanning confocal microscopy. *Mycol Res* **106:**349–354.

134. Eamus D, Thompson W, Cairney JWG, Jennings DH. 1985. Internal structure and hydraulic conductivity of basidiomycete translocating organs. *J Exp Bot* **36:**1110–1116.

135. Cairney JWG. 2005. Basidiomycete mycelia in forest soils: dimensions, dynamics and roles in nutrient distribution. *Mycol Res* **109:**7–20.

136. Duddridge JA, Malibari A, Read DJ. 1980. Structure and function of mycorrhizal rhizomorphs with special reference to their role in water transport. *Nature* **287:**834–836.

137. Granlund HI, Jennings DH, Thompson W. 1985. Translocation of solutes along rhizomorphs of *Armillaria mellea. Trans Br Mycol Soc* **84:**111–119.

138. Tlalka M, Fricker M, Watkinson S. 2008. Imaging of long-distance alpha-aminoisobutyric acid translocation dynamics during resource capture by *Serpula lacrymans. Appl Environ Microbiol* **74:**2700–2708.

139. Brownlee C, Jennings DH. 1982. Long-distance translocation in *Serpula lacrimans:* velocity estimates and the continuous monitoring of induced perturbations. *Trans Br Mycol Soc* **79:**143–148.

140. Lehto T, Zwiazek JJ. 2011. Ectomycorrhizas and water relations of trees: a review. *Mycorrhiza* **21:**71–90.

141. Falconer RE, Bown JL, White NA, Crawford JW. 2007. Biomass recycling: a key to efficient foraging by fungal colonies. *Oikos* **116:**1558–1568.

142. Falconer RE, Bown JL, White NA, Crawford JW. 2005. Biomass recycling and the origin of phenotype in fungal mycelia. *Proc Biol Sci* **272:**1727–1734.

143. Tero A, Takagi S, Saigusa T, Ito K, Bebber DP, Fricker MD, Yumiki K, Kobayashi R, Nakagaki T. 2010. Rules for biologically inspired adaptive network design. *Science* **327:**439–442.

144. Bebber DP, Hynes J, Darrah PR, Boddy L, Fricker MD. 2007. Biological solutions to transport network design. *Proc Biol Sci* **274:**2307–2315.

145. Josefsen L, Droce A, Sondergaard TE, Sørensen JL, Bormann J, Schäfer W, Giese H, Olsson S. 2012. Autophagy provides nutrients for nonassimilating fungal structures and is necessary for plant colonization but not for infection in the necrotrophic plant pathogen *Fusarium graminearum. Autophagy* **8:**326–337.

146. Voigt O, Pöggeler S. 2013. Self-eating to grow and kill: autophagy in filamentous ascomycetes. *Appl Microbiol Biotechnol* **97:**9277–9290.

147. Lindahl B, Finlay R, Olsson S. 2001. Simultaneous, bidirectional translocation of ^{32}P and ^{33}P between wood blocks connected by mycelial cords of *Hypholoma fasciculare. New Phytol* **150:**189–194.

148. Wells JM, Hughes C, Boddy L. 1990. The fate of soil-derived phosphorus in mycelial cord systems of *Phanerochaete velutina* and *Phallus impudicus. New Phytol* **114:**595–606.

149. Wells JM, Boddy L, Donnelly DP. 1998. Wood decay and phosphorus translocation by the cord-forming basidiomycete *Phanerochaete velutina*: the significance of local nutrient supply. *New Phytol* **138:**607–617.

150. Tlalka M, Bebber DP, Darrah PR, Watkinson SC, Fricker MD. 2008. Quantifying dynamic resource allocation illuminates foraging strategy in *Phanerochaete velutina. Fungal Genet Biol* **45:**1111–1121.

151. Tlalka M, Bebber DP, Darrah PR, Watkinson SC, Fricker MD. 2007. Emergence of self-organised oscillatory domains in fungal mycelia. *Fungal Genet Biol* **44:**1085–1095.

152. Connolly JH, Jellison J. 1997. Two-way translocation of cations by the brown rot fungus *Gloeophyllum trabeum. Int Biodeterior Biodegradation* **39:**181–188.

153. Fricker MD, Tlalka M, Bebber D, Takagi S, Watkinson SC, Darrah PR. 2007. Fourier-based spatial mapping of oscillatory phenomena in fungi. *Fungal Genet Biol* **44:**1077–1084.

154. Alim K, Amselem G, Peaudecerf F, Brenner MP, Pringle A. 2013. Random network peristalsis in *Physarum polycephalum* organizes fluid flows across an individual. *Proc Natl Acad Sci USA* **110:**13306–13311.

155. Thompson W, Rayner ADM. 1982. Structure and development of mycelial cord systems of *Phanerochaete laevis* in soil. *Trans Br Mycol Soc* **78:**193–200.

156. Smith ML, Bruhn JN, Anderson JB. 1992. The fungus *Armillaria bulbosa* is among the largest and oldest living organisms. *Nature* **356:**428–431.

157. Ferguson BA, Dreisbach TA, Parks CG, Filip GM, Schmitt CL. 2003. Coarse-scale population structure of pathogenic *Armillaria* species in a mixed-conifer forest in the Blue Mountains of northeast Oregon. *Can J Res* **33:**612–623.

158. Dowson CG, Rayner ADM, Boddy L. 1989. Spatial dynamics and interactions of the woodland fairy ring fungus, *Clitocybe nebularis. New Phytol* **111:**699–705.

159. Rayner ADM. 1997. *Degrees of Freedom: Living in Dynamic Boundaries.* Imperial College Press, London, United Kingdom.

160. Schmid B, Harper JL. 1985. Clonal growth in grassland perennials. 1. Density and pattern-dependent competition between plants with different growth forms. *J Ecol* **73:**793–808.

161. Hutchings MJ, Wijesinghe DK. 1997. Patchy habitats, division of labour and growth dividends in clonal plants. *Trends Ecol Evol* **12:**390–394.

162. Hutchings M, de Kroon H. 1994. Foraging in plants: the role of morphological plasticity in resource acquisition. *Adv Ecol Res* **25:**159–238.

163. Boddy L, Jones TH. 2007. Mycelial responses in heterogeneous environments: parallels with macroorganisms, p 112–158. *In* Gadd G, Watkinson SC, Dyer P (ed), *Fungi in the Environment*, vol 25. Cambridge University Press, Cambridge, United Kingdom.

164. Agerer R. 2001. Exploration types of ectomycorrhizae: a proposal to classify ectomycorrhizal mycelial systems according to their patterns of differentiation and putative ecological importance. *Mycorrhiza* **11:**107–114.

165. Bell AD. 1984. Dynamic morphology: a contribution to plant population ecology, p 31–47. *In* Dirzo R, Sarukhan J (ed), *Perspectives on Plant Population Ecology.* Sinauer Associates Inc, Sunderland, MA.

166. Bell A. 1976. Computerized vegetative mobility in rhizomatous plants, p 3–14. *In* Lindenmayer A, Rozenberg G (ed), *Automata, Languages, Development.* North-Holland Publishing Co, Amsterdam, The Netherlands.

167. Rayner ADM, Franks NR. 1987. Evolutionary and ecological parallels between ants and fungi. *Trends Ecol Evol* **2:**127–133.

168. Dowson CG, Rayner ADM, Boddy L. 1986. Outgrowth patterns of mycelial cord-forming Basidiomycetes from and between woody resource units in soil. *J Gen Microbiol* **132:**203–211.

169. Boddy L, Wood J, Redman E, Hynes J, Fricker MD. 2010. Fungal network responses to grazing. *Fungal Genet Biol* **47:**522–530.

170. Wood J, Tordoff GM, Jones TH, Boddy L. 2006. Reorganization of mycelial networks of *Phanerochaete velutina* in response to new woody resources and collembola (*Folsomia candida*) grazing. *Mycol Res* **110:** 985–993.

171. Olsson S, Hansson BS. 1995. Action potential-like activity found in fungal mycelia is sensitive to stimulation. *Naturwissenschaften* **82:**30–31.

172. Olsson S. 1999. Nutrient translocation and electrical signalling in mycelia, p 25–48. *In* Gow NAR, Robson GD, Gadd GM (ed), *The Fungal Colony*. Cambridge University Press, Cambridge, United Kingdom.

173. Vidal-Diez de Ulzurrun G, Baetens JM, Van den Bulcke J, Lopez-Molina C, De Windt I, De Baets B. 2015. Automated image-based analysis of spatio-temporal fungal dynamics. *Fungal Genet Biol* **84:**12–25.

174. Ritz K, Millar SM, Crawford JW. 1996. Detailed visualisation of hyphal distribution in fungal mycelia growing in heterogeneous nutritional environments. *J Microbiol Methods* **25:**23–28.

175. Hitchcock D, Glasbey CA, Ritz K. 1996. Image analysis of space-filling by networks: application to a fungal mycelium. *Biotechnol Tech* **10:**205–210.

176. Cox PW, Paul GC, Thomas CR. 1998. Image analysis of the morphology of filamentous micro-organisms. *Microbiology* **144:**817–827.

177. Barry DJ, Williams GA. 2011. Microscopic characterisation of filamentous microbes: towards fully automated morphological quantification through image analysis. *J Microsc* **244:**1–20.

178. Spohr A, Dam-Mikkelsen C, Carlsen M, Nielsen J, Villadsen J. 1998. On-line study of fungal morphology during submerged growth in a small flow-through cell. *Biotechnol Bioeng* **58:**541–553.

179. Fuhr MJ, Stührk C, Schubert M, Schwarze FWMR, Herrmann HJ. 2012. Modelling the effect of environmental factors on the hyphal growth of the basidiomycete *Physisporinus vitreus*. *J Basic Microbiol* **52:**523–530.

180. Tucker KG, Kelly T, Delgrazia P, Thomas CR. 1992. Fully-automatic measurement of mycelial morphology by image analysis. *Biotechnol Prog* **8:**353–359.

181. Ritz K, Crawford J. 1990. Quantification of the fractal nature of colonies of *Trichoderma viride*. *Mycol Res* **94:**1138–1141.

182. Barry DJ, Chan C, Williams GA. 2009. Morphological quantification of filamentous fungal development using membrane immobilization and automatic image analysis. *J Ind Microbiol Biotechnol* **36:**787–800.

183. Cross D, Kenerley CM. 2004. Modelling the growth of *Trichoderma virens* with limited sampling of digital images. *J Appl Microbiol* **97:**486–494.

184. Bailey DJ, Thornton CR, Dewey FM, Gilligan CA. 2001. A non-destructive immunoblotting technique for visualisation and analysis of the growth dynamics of *Rhizoctonia solani*. *Mycol Res* **105:**983–990.

185. Nopharatana M, Mitchell DA, Howes T. 2003. Use of confocal scanning laser microscopy to measure the concentrations of aerial and penetrative hyphae during growth of *Rhizopus oligosporus* on a solid surface. *Biotechnol Bioeng* **84:**71–77.

186. Nopharatana M, Mitchell DA, Howes T. 2003. Use of confocal microscopy to follow the development of penetrative hyphae during growth of *Rhizopus oligosporus* in an artificial solid-state fermentation system. *Biotechnol Bioeng* **81:**438–447.

187. Boddy L, Wells JM, Culshaw C, Donnelly DP. 1999. Fractal analysis in studies of mycelium in soil. *Geoderma* **88:**301–328.

188. Boddy L, Donnelly DP. 2008. Fractal geometry and microorganisms in the environment, p 239–272. *In* Senesi N, Wilkinson KJ (ed), *Biophysical Chemistry of Fractal Structures and Processes in Environmental Systems*, vol 11. John Wiley, Chichester, United Kingdom.

189. Karperien A. 2007. FracLac for ImageJ. http://rsb.info.nih.gov/ij/plugins/fraclac/FLHelp/Introduction.htm 1999–2013.

190. Donnelly DP, Boddy L. 2001. Mycelial dynamics during interactions between *Stropharia caerulea* and other cord-forming, saprotrophic basidiomycetes. *New Phytol* **151:**691–704.

191. Baum T, Navarro-Quezada A, Knogge W, Douchkov D, Schweizer P, Seiffert U. 2011. HyphArea—automated analysis of spatiotemporal fungal patterns. *J Plant Physiol* **168:**72–78.

192. Barry DJ, Williams GA, Chan C. 2015. Automated analysis of filamentous microbial morphology with AnaMorf. *Biotechnol Prog* **31:**849–852.

193. Obara B, Grau V, Fricker MD. 2012. A bioimage informatics approach to automatically extract complex fungal networks. *Bioinformatics* **28:**2374–2381.

194. Dirnberger M, Kehl T, Neumann A. 2015. NEFI: Network Extraction From Images. *Sci Rep* **5:**15669.

195. Frangi A, Niessen W, Vincken K, Viergever M. 1998. Multiscale vessel enhancement filtering, p 130–137. *In* Wells W, Colchester A, Delp S (ed), *Medical Image Computing and Computer-Assisted Intervention*, vol 1496. Springer, Berlin, Germany.

196. Basu S, Liu C, Rohde GK. 2015. Localizing and extracting filament distributions from microscopy images. *J Microsc* **258:**13–23.

197. Lopez-Molina C, Vidal-Diez de Ulzurrun G, Baetens JM, Van den Bulcke J, De Baets B. 2015. Unsupervised ridge detection using second order anisotropic Gaussian kernels. *Signal Process* **116:**55–67.

198. Obara B, Fricker M, Gavaghan D, Grau V. 2012. Contrast-independent curvilinear structure detection in biomedical images. *IEEE Trans Image Process* **21:**2572–2581.

199. Fricker M, Boddy L, Nakagaki T, Bebber DP. 2009. Adaptive Biological Networks, p 51–70. *In* Gross T, Sayama H (ed), *Adaptive Networks: Theory, Models and Applications*. Springer, Berlin, Germany.

200. Fricker MD, Lee JA, Bebber DP, Tlalka M, Hynes J, Darrah PR, Watkinson SC, Boddy L. 2008. Imaging complex nutrient dynamics in mycelial networks. *J Microsc* **231:**317–331.

201. Fricker MD, Boddy L, Bebber DP. 2007. Network organisation of mycelial fungi, p 309–330. *In* Howard RJ, Gow NAR (ed), *The Mycota*, vol VIII. Springer-Verlag, Berlin, Germany.

202. Fricker MD, Lee JA, Boddy L, Bebber DP. 2008. The interplay between structure and function in fungal networks. *Topologica* **1:**004.

203. Lamour A, Termorshuizen AJ, Volker D, Jeger MJ. 2007. Network formation by rhizomorphs of *Armillaria lutea* in natural soil: their description and ecological significance. *FEMS Microbiol Ecol* **62:**222–232.

204. Onnela JP, Fenn DJ, Reid S, Porter MA, Mucha PJ, Fricker MD, Jones NS. 2012. Taxonomies of networks from community structure. *Phys Rev E* **86:**036104.

205. Lee SH, Fricker MD, Porter MA. 2017. Mesoscale analyses of fungal networks as an approach for quantifying phenotypic traits. *J Complex Netw* **5:**145–159. doi:10.1093/comnet/cnv034.

206. Goriely A, Tabor M. 2008. Mathematical modeling of hyphal tip growth. *Fungal Biol Rev* **22:**77–83.

207. Sugden KEP, Evans MR, Poon WCK, Read ND. 2007. Model of hyphal tip growth involving microtubule-based transport. *Phys Rev E Stat Nonlin Soft Matter Phys* **75:**031909.

208. Bezzi M, Ciliberto A. 2004. Mathematical modelling of filamentous microorganisms. https://arxiv.org/abs/q-bio/0402004.

209. Gierz G, Bartnicki-Garcia S. 2001. A three-dimensional model of fungal morphogenesis based on the vesicle supply center concept. *J Theor Biol* **208:**151–164.

210. Bartnicki-Garcia S, Bartnicki DD, Gierz G, López-Franco R, Bracker CE. 1995. Evidence that Spitzenkörper behavior determines the shape of a fungal hypha: a test of the hyphoid model. *Exp Mycol* **19:**153–159.

211. Bartnicki-Garcia S, Hergert F, Gierz G. 1989. Computer-simulation of fungal morphogenesis and the mathematical basis for hyphal (tip) growth. *Protoplasma* **153:**46–57.

212. **Wessels JGH.** 1993. Tansley Review 45: Wall growth, protein excretion and morphogenesis in fungi. *New Phytol* **123**:397–413.

213. **Eggen E, Niels de Keijzer M, Mulder BM.** 2011. Self-regulation in tip-growth: the role of cell wall ageing. *J Theor Biol* **283**:113–121.

214. **Parnell S, Gilligan CA, Lucas JA, Bock CH, van den Bosch F.** 2008. Changes in fungicide sensitivity and relative species abundance in *Oculimacula yallundae* and *O. acuformis* populations (eyespot disease of cereals) in Western Europe. *Plant Pathol* **57**:509–517.

215. **Lamour A, Van den Bosch F, Termorshuizen AJ, Jeger MJ.** 2000. Modelling the growth of soil-borne fungi in response to carbon and nitrogen. *IMA J Math Appl Med Biol* **17**:329–346.

216. **Edelstein L.** 1982. The propagation of fungal colonies: a model for tissue-growth. *J Theor Biol* **98**:679–701.

217. **Lopez JM, Jensen HJ.** 2002. Generic model of morphological changes in growing colonies of fungi. *Phys Rev EStat Nonlin Soft Matter Phys* **65**:021903.

218. **Matsuura S.** 2002. Colony patterning and collective hyphal growth of filamentous fungi. *Physica A* **315**:125–136.

219. **Boddy L, Hynes J, Bebber DP, Fricker MD.** 2009. Saprotrophic cord systems: dispersal mechanisms in space and time. *Mycoscience* **50**:9–19.

220. **Deutsch A, Dress A, Rensing L.** 1993. Formation of morphological differentiation patterns in the ascomycete *Neurospora crassa*. *Mech Dev* **44**:17–31.

221. **Crawford JW, Ritz K, Young IM.** 1993. Quantification of fungal morphology, gaseous transport and microbial dynamics in soil: an integrated framework utilizing fractal geometry. *Geoderma* **56**:157–172.

222. **Bolton RG, Boddy L.** 1993. Characterization of the spatial aspects of foraging mycelial cord systems using fractal geometry. *Mycol Res* **97**:762–768.

223. **Jones CL, Lonergan GT, Mainwaring DE.** 1993. Mycelial fragment size distribution: an analysis based on fractal geometry. *Appl Microbiol Biotechnol* **39**:242–249.

224. **Regalado CM, Crawford JW, Ritz K, Sleeman BD.** 1996. The origins of spatial heterogeneity in vegetative mycelia: a reaction-diffusion model. *Mycol Res* **100**:1473–1480.

225. **Orbach R.** 1986. Dynamics of fractal networks. *Science* **231**:814–819.

226. **Nieminen L, Webb S, Smith MCM, Hoskisson PA.** 2013. A flexible mathematical model platform for studying branching networks: experimentally validated using the model actinomycete, *Streptomyces coelicolor*. *PLoS ONE* **8**:e54316.

227. **Boswell GP, Davidson FA.** 2012. Modelling hyphal networks. *Fungal Biol Rev* **26**:30–38.

228. **Jennings L, Watkinson SC.** 1982. Structure and development of mycelial strands in *Serpula lacrimans*. *Trans Br Mycol Soc* **78**:465–474.

229. **Lindahl BJ, Olsson S.** 2004. Fungal translocation: creating and responding to environmental heterogeneity. *Mycologist* **18**:79–88.

230. **Darrah PR, Fricker MD.** 2014. Foraging by a wood-decomposing fungus is ecologically adaptive. *Environ Microbiol* **16**:118–129.

231. **Money NP.** 1990. Measurement of hyphal turgor. *Exp Mycol* **14**:416–425.

232. **Pajor R, Falconer R, Hapca S, Otten W.** 2010. Modelling and quantifying the effect of heterogeneity in soil physical conditions on fungal growth. *Biogeosciences* **7**:3731–3740.

233. **Falconer RE, Bown JL, McAdam E, Perez-Reche P, Sampson AT, van den Bulcke J, White NA.** 2010. Modelling fungal colonies and communities: challenges and opportunities. *IMA Fungus* **1**:155–159.

234. **West GB, Savage VM, Gillooly J, Enquist BJ, Woodruff WH, Brown JH.** 2003. Physiology: why does metabolic rate scale with body size? *Nature* **421**:713, discussion 714.

235. **Banavar JR, Maritan A, Rinaldo A.** 1999. Size and form in efficient transportation networks. *Nature* **399**:130–132.

236. **Maritan A, Colaiori F, Flammini A, Cieplak M, Banavar JR.** 1996. Universality classes of optimal channel networks. *Science* **272**:984–986.

237. **Katifori E, Szöllosi GJ, Magnasco MO.** 2010. Damage and fluctuations induce loops in optimal transport networks. *Phys Rev Lett* **104**:048704.

238. **Boddy L, Jones TH.** 2008. Interactions between Basidiomycota and invertebrates, p 155–179. *In* Boddy L, Frankland JC, West P (ed), *Ecology of Saprotrophic Basidiomycetes*. Elsevier, Amsterdam, The Netherlands.

239. **Crowther TW, Jones TH, Boddy L.** 2012. Interactions between saprotrophic basidiomycete mycelia and mycophagous soil fauna. *Mycology* **3**:77–86.

240. **A'Bear AD, Jones TH, Boddy L.** 2014. Size matters: what have we learnt from microcosm studies of decomposer fungus-invertebrate interactions? *Soil Biol Biochem* **78**:274–283.

241. **Tordoff GM, Boddy L, Jones TH.** 2006. Grazing by *Folsomia candida* (Collembola) differentially affects mycelial morphology of the cord-forming basidiomycetes *Hypholoma fasciculare*, *Phanerochaete velutina* and *Resinicium bicolor*. *Mycol Res* **110**:335–345.

242. **Crowther TW, Boddy L, Jones TH.** 2011. Outcomes of fungal interactions are determined by soil invertebrate grazers. *Ecol Lett* **14**:1134–1142.

243. **Rotheray TD, Jones TH, Fricker MD, Boddy L.** 2008. Grazing alters network architecture during interspecific mycelial interactions. *Fungal Ecol* **1**:124–132.

244. **Rotheray TD, Boddy L, Jones TH.** 2009. Collembola foraging responses to interacting fungi. *Ecol Entomol* **34**:125–132.

245. **Nuss DL.** 2011. Mycoviruses, RNA silencing, and viral RNA recombination. *Adv Virus Res* **80**:25–48.

246. **Ghabrial SA, Castón JR, Jiang D, Nibert ML, Suzuki N.** 2015. 50-plus years of fungal viruses. *Virology* **479–480**:356–368.

247. **Van den Bulcke J, Masschaele B, Dierick M, Acker JV, Stevens M, Hoorebeke LV.** 2008. Three-dimensional imaging and analysis of infested coated wood with X-ray submicron CT. *Int Biodeterior Biodegradation* **61**:278–286.

248. **Van den Bulcke J, Boone M, Van Acker J, Van Hoorebeke L.** 2009. Three-dimensional X-ray imaging and analysis of fungi on and in wood. *Microsc Microanal* **15**:395–402.

249. **Lilje O, Lilje E, Marano AV, Gleason FH.** 2013. Three dimensional quantification of biological samples using micro-computer aided tomography (microCT). *J Microbiol Methods* **92**:33–41.

250. **Sedighi Gilani M, Boone MN, Mader K, Schwarze FWMR.** 2014. Synchrotron X-ray micro-tomography imaging and analysis of wood degraded by *Physisporinus vitreus* and *Xylaria longipes*. *J Struct Biol* **187**:149–157.

251. **Dickson S, Kolesik P.** 1999. Visualisation of mycorrhizal fungal structures and quantification of their surface area and volume using laser scanning confocal microscopy. *Mycorrhiza* **9**:205–213.

252. **Vierheilig H, Schweiger P, Brundrett M.** 2005. An overview of methods for the detection and observation of arbuscular mycorrhizal fungi in roots. *Physiol Plant* **125**:393–404.

253. **Vierheilig H, Knoblauch M, Juergensen K, van Bel AJE, Grundler FMW, Piché Y.** 2001. Imaging arbuscular mycorrhizal structures in living roots of *Nicotiana tabacum* by light, epifluorescence, and confocal laser scanning microscopy. *Can J Bot* **79**:231–237.

254. **Knaus H, Blab GA, Jerre van Veluw G, Gerritsen HC, Wösten HAB.** 2013. Label-free fluorescence microscopy in fungi. *Fungal Biol Rev* **27**:60–66.

255. **Vági P, Knapp DG, Kósa A, Seress D, Horváth ÁN, Kovács GM.** 2014. Simultaneous specific in planta visualization of root-colonizing fungi using fluorescence in situ hybridization (FISH). *Mycorrhiza* **24**:259–266.

256. **Rath M, Grolig F, Haueisen J, Imhof S.** 2014. Combining microtomy and confocal laser scanning microscopy for structural analyses of plant-fungus associations. *Mycorrhiza* **24**:293–300.

257. Melville L, Dickson S, Farquhar ML, Smith SE, Peterson RL. 1998. Visualization of mycorrhizal fungal structures in resin embedded tissues with xanthene dyes using laser scanning confocal microscopy. *Can J Bot* **76:**174–178.

258. Giovannetti M, Fortuna P, Citernesi AS, Morini S, Nuti MP. 2001. The occurrence of anastomosis formation and nuclear exchange in intact arbuscular mycorrhizal networks. *New Phytol* **151:**717–724.

259. Giovannetti M, Sbrana C, Avio L, Strani P. 2004. Patterns of belowground plant interconnections established by means of arbuscular mycorrhizal networks. *New Phytol* **164:**175–181.

260. Czymmek KJ, Bourett TM, Sweigard JA, Carroll A, Howard RJ. 2002. Utility of cytoplasmic fluorescent proteins for live-cell imaging of *Magnaporthe grisea* in planta. *Mycologia* **94:**280–289.

261. Czymmek KJ, Bourett TM, Howard RJ. 2004. Fluorescent protein probes in fungi. *Methods Microbiol* **34:**27–62.

262. Hickey PC, Swift SR, Roca MG, Read ND. 2005. Live-cell imaging of filamentous fungi using vital fluorescent dyes and confocal microscopy, p 63–87. *In Methods in Microbiology*, vol 34, *Microbial Imaging*. Elsevier, Amsterdam, The Netherlands.

263. Pringle A, Taylor J. 2002. The fitness of filamentous fungi. *Trends Microbiol* **10:**474–481.

264. Gilchrist MA, Sulsky DL, Pringle A. 2006. Identifying fitness and optimal life-history strategies for an asexual filamentous fungus. *Evolution* **60:**970–979.

265. Cairney JWG, Jennings DH, Veltkamp CJ. 1989. A scanning electron-microscope study of the internal structure of mature linear mycelial organs of four basidiomycete species. *Can J Bot* **67:**2266–2271.